SLAC-PUB-1123
(TH) and (EXP)
September 1972

Amplitude Structure in Pseudoscalar-Meson Baryon Scattering*

J.A.J. Matthews

Stanford Linear Accelerator Center
Stanford University, Stanford, California 94305

ABSTRACT

Recent analyses are reviewed that determine the amplitude structure of meson baryon scattering directly from the data. Harari's explanation of the "crossover" effect in elastic scattering is introduced, motivating the evaluation of ω^o and f^o exchange amplitudes from the data. Uncertainties in the analysis of the f^o amplitude are detailed, and are noted to arise from the uncertainty in the pomeron contribution to elastic scattering. Finally, the dual absorptive model (DAM) of Harari is presented and compared to data on charge exchange and strangeness exchange reactions. Particular emphasis is placed on the comparison of the DAM to the crossed reactions $\pi p \to K(\Lambda,\Sigma)$ and $\bar{K}p \to \pi(\Lambda,\Sigma)$.

(Talk presented at: Canadian Institute of Particle Physics Summer School, McGill University, August 28-September 2, 1972)

---

* Work supported by the U.S. Atomic Energy Commission

1. Introduction

With the beginning of experiments in the hundreds of GeV/c region at NAL, it would seem an appropriate time to summarize our knowledge of scattering amplitudes in the few GeV/c momentum region. Our discussion will focus on analysis techniques applicable at higher energies, and in particular with the observation by Harari[1] that certain helicity amplitudes can be simply determined from elastic scattering data.

Recently there has been a growing interest in the possibility of determining the structure of two body helicity amplitudes directly from the experimental data. Generally a complete determination of the scattering amplitudes in a model independent analysis requires the measurement of the differential cross section, polarization and at least some elements of the depolarization tensor for that process.[2] This has in fact been done at 6 GeV/c for πp scattering,[3] but typically requires a prohibitively excessive experimental effort.

The approach to extract the imaginary part of the s-channel helicity nonflip amplitude, Im $R_{\Delta\lambda=0}(s,t)$ suggested by Harari[1] is therefore of particular interest due to its simplicity. In Sect. 2 these ideas are reviewed, and applied to recent elastic scattering data.[4-6] The different viewpoints on the determination of the f^o exchange amplitude[7-11] are elaborated and are found to result from our lack of understanding of the pomeron contribution to elastic scattering. The importance of the new data on $\gamma p \to \phi p$[12] is discussed. This section closes with a brief comment on the relation of "peripheral" exchange amplitudes in duality.

In Sect. 3 the dual absorptive model (DAM) of Harari is introduced,[13] and compared to a number of pseudoscaler-meson baryon scattering processes. This later work is presented in detail elsewhere[14]; the accent in the present discussion will be on the crossed pairs of reactions:

$$\pi p \to K \Sigma \qquad (1)$$
$$\bar{K} p \to \pi \Sigma$$

and

$$\pi p \to K \Lambda \qquad (2)$$
$$\bar{K} p \to \pi \Lambda$$

A compilation of the data for these reactions has been made,[14-16] and is related to the predictions of exchange degeneracy.

Finally, Sect. 4 contains a summary.

2. Amplitude Review

(a) The crossover phenomenon.

In pseudoscaler-meson baryon scattering there are two helicity amplitudes:

$R_{\Delta\lambda=0}(s,t)$, the s channel nonflip amplitude,

and $R_{\Delta\lambda=1}(s,t)$, the s channel helicity flip amplitude.

The differential cross section for $K^{\pm}p$ elastic scattering can therefore be written as:

$$\left(\frac{d\sigma}{dt}\right)_{K^{\pm}p} = \sum_{\Delta\lambda=0,1} \left| P_{\Delta\lambda} + R_{\Delta\lambda}^{(\text{even})} \pm R_{\Delta\lambda}^{(\text{odd})} \right|^2 \qquad (3)$$

Where $P_{\Delta\lambda}$ is the pomeron contribution, and $R_{\Delta\lambda}^{\binom{\text{even}}{\text{odd}}}$ is the contribution from

($\overset{\text{even}}{\text{odd}}$) Regge exchanges. Since the pomeron dominates the Regge contribution in elastic scattering, is predominantly imaginary and s-channel helicity conserving[17], Harari notes that Eqn. 3 reduces to the simple form:

$$\left(\frac{d\sigma}{dt}\right)_{K^-p} \approx P^2_{\Delta\lambda=0} + 2P_{\Delta\lambda=0}\ \text{Im}\ R_{\Delta\lambda=0} \qquad (4)$$

$$\left(\frac{d\sigma}{dt}\right)_{K^+p} \approx P^2_{\Delta\lambda=0}$$

In Eqn. 4 Regge squared terms have been neglected, and from duality it is assumed that the Regge exchange contribution is predominatly real in the exotic K^+p channel. The K^+p data therefore "isolates" the pomeron amplitude, and allows the crossing odd Regge contribution to be determined directly from the data:

$$\text{Im}\ R^{(\text{odd})}_{\Delta\lambda=0} \approx \frac{\left(\frac{d\sigma}{dt}\right)_{K^-p} - \left(\frac{d\sigma}{dt}\right)_{K^+p}}{2\sqrt{\left(\frac{d\sigma}{dt}\right)_{K^+p}}} \qquad (5)$$

An example of the data[5] for these reactions is shown in Fig. 1. The K^-p cross section is seen to be larger than the K^+p at t=0, but is equal to the K^+p cross section for $-t \approx 0.2\ \text{GeV}^2$. Harari interprets the "crossover", following Eqn. 5, as a zero in the imaginary part of the helicity nonflip Regge amplitude in elastic scattering.

A similar analysis is also applicable to the pp and $\bar{p}p$ elastic scattering data, where the pp channel is exotic. It is interesting to note that an analogous effect also occurs in diffraction dissociation data, where a crossover has been observed in $Kp \to Qp$ and $\bar{K}p \to \bar{Q}p$ data[18], see Fig. 2,

and in the reactions $\pi^{\pm}p \rightarrow A_1^{\pm}p$.[19] This latter data suggests that Regge as well as pomeron contributions are important to the "diffractive" production of multiparticle final states.

The determination of the helicity amplitude Im $R^{(odd)}_{\Delta\lambda=0}$ has been done by Davier and Harari[4] at 5 GeV/c, see Fig. 3, and by other groups.[5,6] All analyses fit the data with the Bessel function form motivated by geometrical-optical models:

$$\text{Im } R_{\Delta\lambda=0}(t) \approx J_o(r\sqrt{-t}\,)\, e^{At} \tag{6}$$

yielding results for the interaction radius of $r \approx 5$ GeV^{-1} and for the slope parameter of $A \approx 1.0$ GeV^{-2}. This analysis can also be considered in impact parameter space:

$$\text{Im } \tilde{R}_{\Delta\lambda=0}(b) \approx \int_o^{t_{max}} \text{Im } R_{\Delta\lambda=0}(t)\;\; J_o(b\sqrt{-t})\;\sqrt{-t}\; dt \tag{7}$$

The distribution at 5 GeV/c in impact parameter space is shown in Fig. 4, and is observed to be dominated by peripheral partial waves. Qualitatively elastic scattering can be considered to be composed of two parts: the pomeron, which is absorptive and is the result of the "shadow" of other processes; and the Regge exchange contribution, which is presumably peripheral as a result of the diminished probability for a given scattering process to occur for small values of the impact parameter.

Parenthetically we note that the elastic polarization ($\mathscr{P}$) is given by:

$$\mathscr{P} \approx -2(P_{\Delta\lambda=0}\, \text{Re}R_{\Delta\lambda=1})/(\frac{d\sigma}{dt}) \tag{8}$$

allowing another part of the helicity amplitude structure to be determined:

$$\text{Re } R^{\binom{\text{even}}{\text{odd}}}_{\Delta\lambda=1} \approx \frac{\mathcal{P}\left(\frac{d\sigma}{dt}\right)_{K^+p} \pm \mathcal{P}\left(\frac{d\sigma}{dt}\right)_{K^-p}}{4\sqrt{\left(\frac{d\sigma}{dt}\right)_{K^+p}}} \tag{9}$$

An example of such a separation is shown in Fig. 5. The data look remarkably like the predictions of simple Regge pole models for A_2 and ρ exchange:

$$\text{Re } R^{\binom{\text{even}}{\text{odd}}}_{\Delta\lambda=1} \approx \sqrt{-t}\, e^{Bt} \begin{pmatrix} \cos^2\left[\pi\, \alpha\,(t)/2\right] \\ \sin^2\left[\pi\alpha\,(t)/2\right] \end{pmatrix} \tag{10}$$

where $\alpha(t) \approx 0.5 + 0.9\ t$. This observation, plus the fact that Regge and geometrical model predictions for $\text{Im } R^{\binom{\text{even}}{\text{odd}}}_{\Delta\lambda=1}$ are essentially equivalent (and in agreement with the data) suggests that:

$$\text{Im } R^{\binom{\text{even}}{\text{odd}}}_{\Delta\lambda=1} \approx J_1\left(r\sqrt{-t}\right) e^{At}, \tag{11}$$

similar to the helicity nonflip amplitude (see Eqn. 6).

(b) The f^o amplitude debate.

In contrast to the relative simplicity of obtaining the helicity amplitude $\text{Im } R^{(\text{odd})}_{\Delta\lambda=0}$ from the data, see Eqn. 5, the evaluation of the f^o amplitude, $\text{Im } R^{(\text{even})}_{\Delta\lambda=0}$, has met with considerable controversy. The analyses tend to fall into two camps, the peripheralists and the non-peripheralists. We will first review the peripheralists.

(i) Gordon, Lai and Paige: This analysis[7] attempts to determine the zero structure of the f^o amplitude, "f(t)", by considering the combination of elastic scattering cross sections:

$$\text{"f(t)"} \approx \left(\frac{\frac{d\sigma}{dt}(\bar{X}p) + \frac{d\sigma}{dt}(Xp)}{2\, s^{\alpha_p(t)-1} \sqrt{\frac{d\sigma}{dt}(Xp)}} \right)_{P_{LAB_1}} - \left(\text{same} \right)_{P_{LAB_2}} \qquad (12)$$

where Xp, and $\bar{X}p$ are the particle and antiparticle reactions, and $\alpha_p(t)$ is the effective "pomeron" trajectory determined from elastic pp data. The s^{α_p-1} in the denominator of Eqn. 12 factors out the energy dependence of the pure pomeron contribution, $P_{\Delta\lambda=0} \sim \sqrt{\frac{d\sigma}{dt}(Xp)}$, see Eqn. 4, so that this contribution can be removed by subtraction at two different energies. This technique does yield a zero in the crossing even Regge contribution at $-t \approx 0.15$ GeV^2, but the authors do not discuss the uncertainties in this value resulting from their assumptions for the pomeron amplitude.

(ii) Davier: Davier[8] approaches the problem by assuming a fixed model for pomeron and f^o amplitudes:

$$\begin{aligned} P_{\Delta\lambda=0} &= i\, A_p\, e^{B_p t} \\ \text{Im}\, f_{\Delta\lambda=0} &= A_f\, J_o(r_f \sqrt{-t})\, e^{B_f t} \end{aligned} \qquad (13)$$

The parameters A_p and A_f are then determined from total cross section data, and take the form:

$$\left.\begin{aligned} A_p &= 4.82 \pm 0.14 \\ A_f &= (5.41 \pm 0.46)\ s^{-(0.56 \pm 0.08)} \end{aligned}\right\} \ \text{mb}^{1/2}/\text{GeV} \qquad (14)$$

The sum of $\pi^{\pm}p$ elastic differential cross sections are then fitted at each energy to determine the remaining three parameters. The data are well fitted[8], and yield the results for B_p, B_f and r_f shown in Fig. 6 and 7.

Davier's analysis implies that the pomeron diffraction peak shrinks, and with a rate dependent on energy. A similar effect is observed in elastic pp data,[20] see Fig. 8, which shows the largest shrinkage at low energies. Perhaps this reveals that the pomeron is being "built up" from the opening of inelastic channels. Significant changes might therefore be expected in the "pomeron" at low energies. For comparison, Davier[8] represents by the shaded region in Fig. 6 the experimental data on K^+p slopes evaluated in the same t interval, $-t < 0.9$ GeV^2.

The analysis[8] also suggests that the f^o amplitude is peripheral, is of approximately constant radius, $< r_f > \sim 5.2$ GeV^{-1}, and shrinks with a Regge slope $\alpha' \sim 1.1$ GeV^{-2}.

One argument against Davier's analysis is that it uses data out to momentum transfers of $-t \approx 0.9$ GeV^2. In this region the pomeron amplitude may no longer be represented by a single exponential or may have significant real parts or a helicity flip contribution in disagreement with his assumptions, see Eqn. 13. The assumption was also made that the pomeron amplitude at t=0 was energy independent, see Eqn. 14. Relaxation of these requirements was observed to make no significant difference in the results however.[8]

(iii) Chadwick, Eisenberg and Kogan: This analysis[9] essentially duplicates Davier's analysis, but for the reaction $\gamma p \rightarrow \rho^o p$. The data are well reproduced by the parameterization:

$$\left.\begin{aligned} P_{\Delta\lambda=0} &= i\, A_p\, e^{B_p t} \\ \mathrm{Im}\, f_{\Delta\lambda=0} &= \frac{A_f}{\sqrt{s}}\, J_o(r_f \sqrt{-t})\, e^{B_f t} \end{aligned}\right\} \qquad (15)$$

where the energy dependence of the amplitudes has been explicitely included (compare with Eqns. 13 and 14), and $r_f \approx 1$ fm. The results for B_f and B_p are shown in Fig. 9. This presentation of the results is somewhat of an overstatement however, since these results were obtained only after preliminary energy dependent fits were made, assuming Regge shrinkage ($B \approx B_o + \alpha' \ell ns$), to determine the best values of A_f and A_p. Nevertheless a consistent interpretation of the data is obtained, and the pomeron slope, B_p, is observed to agree with the results of Davier[8] (dashed line in Fig. 9.)

It is also observed that the pomeron slope obtained from the $\gamma\, p \to \rho^o p$ data is in good agreement with the slope of $\gamma\, p \to \phi\, p$ data,[21,22] where only the pomeron is thought to contribute[23]. Interestingly, the most recent measurement of the slope for ϕ photoproduction by Ritson, Prepost et al.[12] finds no shrinkage of the forward peak ($\alpha'_p = -0.03 \pm 0.13$) in the interval of photon energies 6 to 19 GeV! This result would contradict low energy data on $\gamma\, p \to \phi\, p$[22] if it is also true that the pomeron does not shrink below 6 GeV. However, the result is not in disagreement with other data in the same energy interval.

The Ritson-Prepost, et al.[12] data are measured at 12 GeV for $0.2 \leq -t \leq 1.0$ GeV^2, and at $-t = 0.6$ GeV^2 for $6 \leq E_\gamma \leq 19$ GeV. The results of these measurements are shown in Figs. 10 and 11. The data at 12 GeV are observed to be in agreement with both curves in Fig. 10, although the data at large

momentum transfers are not well represented by a single exponential. In contrast, the K^+p elastic differential cross section, also thought to be pomeron dominated, is well represented by a single exponential for $-t \leq 1.0$ GeV^2 and for momenta $P_{LAB} \gtrsim 5$ GeV/c[24]. The band of values plotted in Fig. 9 represents the spread of slopes for ϕ photoproduction consistent with the two curves in Fig. 10.

The constant cross section for $\gamma p \to \phi p$ at $-t = 0.6$ GeV^2, see Fig. 11, implies no shrinkage for this reaction. This result is quite insensitive to an energy dependence to the forward cross section. In particular assuming an optimistic energy dependence compatible with the apparent growth of the K^+p total cross section[25] results in an increase in the shrinkage parameter for the $\gamma p \to \phi p$ data to $\alpha'_p \approx 0.1$ GeV^{-2}. For comparison, in the same energy region the pomeron shrinkage in elastic K^+p data or from the analysis of $\pi^{\pm}p$ data by Davier[8] yields a value of $\alpha'_p \approx 0.6$ GeV^{-2}.

Barger and coworkers[10,11] have championed the non-peripheralist point of view for the f^o exchange amplitude. In particular Barger, Geer, and Halzen[11] find that if the pomeron shrinks at a fixed (energy independent) rate, then for $\alpha'_p \lesssim 0.4$ GeV^{-2} the Kp and πp elastic scattering data are inconsistent with the amplitude Im $R^{(even)}_{\Delta\lambda=0}$ being peripheral, as shown in Fig. 12. If α'_p is in fact energy independent it should be given by asymptotic pp scattering data. Choosing the ISR value, $0.15 < \alpha'_p < 0.35$ GeV^{-2},[27] which is also consistent with the Ritson-Prepost $\gamma p \to \phi p$ result, then implies that the f^o amplitude is not peripheral.

The observation of Barger et al[11] that the evaluation of the f^o amplitude depends sensitively on the rate of pomeron shrinkage also applies to the results of old FESR analyses.[28-30] These analyses typically chose $\alpha'_p \lesssim 0.5$ GeV^{-2}, and found that the f^o amplitude was consistent with having

a zero at $-t \approx 0.4$ GeV^2.[29,30] Such FESR analyses confirm the results of Fig. 12,[11] but provide no additional information on the pomeron rate of shrinkage.

In the light of the conflicting evidence we can only summarize the situation:

(i) if the pomeron shrinks slowly $\left(\alpha_p' < 0.4\right)$, or does not shrink as suggested by the Ritson-Prepost data, or if α_p' is independent of energy so that ISR data can be used, then the f^o amplitude is not consistent with being peripheral; however

(ii) if the $\gamma p \to \phi p$ data is incorrect, or does not depict only the pomeron contribution, and if the pomeron shrinks with an α_p' dependent on energy then the f^o amplitude is consistent with being peripheral.

(c) Duality, EXD and absorbed amplitudes.

As discussed above, the imaginary parts of the crossing odd Regge exchange amplitudes Im $R_{\Delta\lambda}^{(odd)}$, are observed to be peripheral (absorbed). What then does this imply for duality and EXD (exchange degeneracy)? Recently Harari[13] has suggested that for the imaginary parts of the scattering amplitudes, duality relates:

structure in low energy s channel resonances	$\longleftrightarrow$	high energy peripheral amplitudes

This conjecture is graphically displayed in Fig. 13 where the first zeros in the contribution of prominent s-channel resonances to the s-channel

helicity amplitudes occur at approximately fixed value of momentum transfer. For nonflip and flip amplitudes these zeros are at $-t \approx 0.2$ GeV^2 and $-t \approx 0.5$ GeV^2 respectively, in agreement with the zeros of high energy peripheral amplitudes for $r \approx 1$ fm (see Eqns. 6 and 11).

Two points of view can now be taken:

(i) Duality and EXD good. Knowledge that the imaginary parts of crossing odd exchange amplitudes are peripheral then suggests that even exchange amplitudes are also peripheral. Complete cancellation of the imaginary part of the Regge exchange amplitudes for reactions with an exotic s-channel can then occur only if the r and A parameters for the peripheral amplitudes (see Eqns. 6 and 11) are equal for crossing even and odd exchanges.

(ii) Duality and EXD broken. In this case the crossing even amplitudes are not directly related to the odd amplitudes, and need not be peripheral.

3. Comparison of the DAM to Charge Exchange and Strangeness Exchange Reactions.

(a) Introduction

As discussed in the previous section, the crossing odd Regge exchange amplitudes (vector exchanges ρ,ω^9) and possibly also the crossing even Regge exchange amplitudes (tensor exchanges A_2,f^9) are consistent with having peripheral imaginary parts. It was also noted that for the helicity flip amplitudes the simple Regge model predictions were in good agreement with the data.

These features of the data are explicitely included in the dual absorptive model (DAM) of Harari.[13] The suggested form for the s-channel

helicity amplitudes in the DAM in effect summarizes section 2 above:

$$\begin{aligned}
&\text{Im } R_{\Delta\lambda=0}(t) \approx (\pm) J_0(r\sqrt{-t}) e^{At} && \begin{pmatrix}\text{vector}\\ \text{tensor}\end{pmatrix} \\
&\text{Re } R_{\Delta\lambda=0}(t) \approx \quad \text{(unknown)} && \\
&\text{Im } R_{\Delta\lambda=1}(t) \approx (\pm) J_1(r\sqrt{-t}) e^{At} && \begin{pmatrix}\text{vector}\\ \text{tensor}\end{pmatrix} \\
&\text{Re } R_{\Delta\lambda=1}(t) \approx \quad J_1(r\sqrt{-t}) e^{At} \tan\left(\tfrac{1}{2}\pi\alpha(t)\right) && \text{vector} \\
&\qquad\qquad \approx \quad J_1(r\sqrt{-t}) e^{At} \cot\left(\tfrac{1}{2}\pi\alpha(t)\right) && \text{tensor}
\end{aligned} \tag{16}$$

This model is observed to be in qualitative agreement with the data.[13] For a more detailed comparison to the data Jim Loos and myself choose the following parametrical form for the vector exchange amplitudes:[14]

$$\text{Im } R^V_{\Delta\lambda=0}(s,t) = g_0^V \left(\frac{s}{s_0}\right)^{\alpha(t)} J_0(r\sqrt{-t}) e^{A_V t} \tag{17}$$

$$\text{Re } R^V_{\Delta\lambda=0}(s,t) = g_0^V \left(\frac{s}{s_0}\right)^{\alpha(t)} \left[\left(1 + a_V t + b_V t^2, e^{B_V t}\right] \right. \quad e^{A_V t} \tan\left(\tfrac{1}{2}\pi\alpha(0)\right)$$

$$R^V_{\Delta\lambda=1}(s,t) = g_1^V \left(\frac{s}{s_0}\right)^{\alpha(t)} J_1(r\sqrt{-t})\, e^{A_V t} \left(\tan\left(\tfrac{1}{2}\pi\alpha(t)\right) + i\right)$$

and an analogous form for the tensor exchange amplitudes (but with $\tan \leftrightarrow \cot$, etc.). The parameters in the model are:

g_0^V, g_1^V	coupling constants
A_V, B_V	exponential slope parameters
a_V, b_V	polynomial coefficients
r	interaction radius

and we set $s_0 = 1$ GeV, $\alpha(t) = 0.5 + 0.9t$. The amplitudes are chosen

to have Regge energy dependence, and the Regge phase at t = 0. This phase choice agrees with the data on K_S^o regeneration[31] and with the determination of the forward πN charge exchange amplitudes by Höhler and Strauss.[32]

The model was compared to the reactions:

$$\pi^- p \to \pi^o n$$

$$\pi^- p \to \eta^o n$$

$$K_L^o p \to K_S^o p$$

$$K^+ n \to K^o p$$

$$K^- p \to \bar{K}^o n$$

and the agreement with the data was observed to be good, see Figs. 14, 15 for example. The resulting ρ and A_2 amplitudes determined from the data are shown in Fig. 16. Also shown in this figure are the results of the model independent amplitude analysis of Halzen and Michael,[3] shown as the points in Fig. 16(a). The two analyses are observed to give a similar description for the ρ amplitude structure.

The results of the DAM comparisons to the data are:[14]

(i) assuming approximately equal interaction radii for vector and tensor exchanges, $r_\rho \approx r_{A_2}$, then the data are consistent with equal slope parameters, $A_\rho \approx A_{A_2}$, and with the independence of both r and A on the net helicity flip in the reaction:

$$r_{\Delta\lambda=1} \approx r_{\Delta\lambda=0}$$
$$A_{\Delta\lambda=1} \approx A_{\Delta\lambda=0} \qquad (18)$$

Recall that in Sect. 2(c) the simultaneous equality of r and A parameters was required for strong exchange degeneracy to be satisfied for peripheral amplitudes.

The slope parameters, A, determined from the present analysis where helicity flip amplitudes dominate, can also be compared to the results of the amplitude analyses[4-6] described in Sect. 2 that determine the imaginary part of the nonflip amplitudes from elastic scattering data. The results are in agreement with the approximate equalities of Eqn. 18. The equality of r and A parameters for helicity flip and nonflip amplitudes implies that the impact parameter representations of these two amplitudes are similar, at least in the peripheral region $b \gtrsim 1/2$ fm.[14,33]

(ii) The coupling constants obtained for the Kp charge exchange reactions were in good agreement with SU(3) predictions:[14]

$$A(K^- p \to \bar{K}^o n) = -\sqrt{\tfrac{1}{2}}\, A(\pi^- p \to \pi^o n) + \sqrt{3/2}\, A(\pi^- p \to \eta^o n)$$

$$A(K^+ n \to K^o p) = +\sqrt{\tfrac{1}{2}}\, A(\pi^- p \to \pi^o n) + \sqrt{3/2}\, A(\pi^- p \to \eta^o n)$$

Points (i) and (ii) are consistent therefore with strong exchange degeneracy for the amplitudes in the Kp charge exchange reaction.

(b) Strangeness Exchange Reactions

The channels that we study are the pairs of s-u crossed reactions given in Eqns. 1 and 2. The data[14-16] show the following trends for the cross sections and the forward slopes of the differential cross section, B:

$$\sigma(\bar{K}N \to \pi Y) > \sigma(\pi N \to KY)$$

$$B(\pi N \to KY) > B(\bar{K}N \to \pi Y)$$

where Y represents either Σ or Λ^o. Barloutaud's recent compilation of cross sections[16], Fig. 17, suggests that the above inequality holds for all momentum values measured, $P_{LAB} \lesssim 15$ GeV/c.

Assuming the domination of reactions (1) and (2) by K* and K** t channel Regge exchanges, simple Regge-pole models with exchange degenerate trajectories predict:

$$\frac{d\sigma}{dt}(\bar{K}N \to \pi Y) = \frac{d\sigma}{dt}(\pi N \to KY) \qquad (19)$$

in disagreement with the data, see fig. 17. Alternatively, our formulation of

the DAM, Eqn. 17, suggests that the forward differential cross sections may be equal:

$$\left(\frac{d\sigma}{dt}\right)_0 (\bar{K}N \rightarrow \pi Y) \approx \left(\frac{d\sigma}{dt}\right)_0 (\pi N \rightarrow KY) \qquad (20)$$

but that absorption can alter the amplitudes for $t \neq 0$, resulting in:

$$B(\bar{K}N \rightarrow \pi Y) \neq B(\pi N \rightarrow KY).$$

The data for the forward differential cross sections and slopes for the Λ^o channels are shown in Figs. 18 and 19 respectively. The forward cross sections are consistent with equality; the slopes are observed to be substantially different, however.

To see whether the slopes of the crossed reactions do tend toward equality at high energy we can try to estimate the slopes from the total cross section data. Assuming equal forward cross sections, Eqn. 20, and exponential differential cross sections for reactions (1) and (2), see Fig. 20, yields the relation:

$$\frac{\sigma(\bar{K}N \rightarrow \pi Y)}{\sigma(\pi N \rightarrow KY)} \approx \frac{B(\pi N \rightarrow KY)}{B(\bar{K}N \rightarrow \pi Y)}.$$

Barloutaud's compilation, Fig. 17, suggests therefore that the forward slopes in Λ^o production are not rapidly becoming equal at higher energies. As a result the Regge shrinkage predictions in Fig. 19 may provide a good estimate for the forward slopes of these reactions above the energies of existing measurements.[34]

The polarization data for the Σ reactions are shown in Fig. 21. No strong momentum dependence is observed in these data, suggesting again that the Regge factor $(s/s_0)^{\alpha(t)}$ is the dominant energy dependence in the Regge exchange amplitudes.

Duality diagrams[35] suggest that the scattering amplitudes should be purely real in the $\bar{K}N \rightarrow \pi Y$ channel, and the polarization zero. This result is not required by duality, however, since neither reaction (1) or (2) has an

exotic s channel. On examining the data,[14] Fig. 21, we find a substantial polarization in the $\bar{K}N \to \pi Y$ channel in disagreement with the predictions of duality diagrams.

The peripheral and nonperipheral points of view introduced in Sect. 2 now make a return appearance in the analysis of the Λ^o and Σ polarization data. Noting that helicity flip amplitudes are "indistinguishable" between peripheral and simple Regge models, Barger and Martin[36] suggest that the predictions of duality diagrams may only apply to these amplitudes. In this case the polarization, $\mathscr{P}$, for the reactions $\bar{K}N \to \pi Y$ is given by:

$$\mathscr{P} \approx \text{Im } R_{\Delta\lambda=0} \text{ Re } R_{\Delta\lambda=1} \tag{21}$$

In the DAM, with equal radii of interactions for vector and tensor exchanges, this reduces to:

$$\mathscr{P} \approx J_o(r\sqrt{-t}) \text{ Re } R_{\Delta\lambda=1}$$

which has (at least) the $-t \sim 0.2$ GeV^2 zero from the Bessel function. This disagrees with the $\bar{K}N \to \pi Y$ data[14], see Fig. 21. Alternatively, if K* and K** amplitudes have significantly different interaction radii[36] a solution can be found that satisfies Eqn. 21.

In the DAM a solution exists if K* and K** amplitudes in reactions 1 and 2 fail to satisfy strong EXD.[14] This latter result is in contrast, however, with the DAM analysis of KN charge exchange which yields ρ and A_2 amplitudes consistent with strong EXD.

In summary, the nonperipheralists would suggest that at present energies the s-channel helicity nonflip amplitudes do not satisfy strong EXD. This implies, however, that the amplitudes in K^+n charge exchange have imaginary parts despite the fact that the s-channel for this reaction is exotic.

Alternatively, the peripheralists are consistent with duality, but must break SU(3) between the ρ and A_2 trajectories, and between the K* and K** trajectories. For additional discussion see ref. 14.

4. Summary

From the review of amplitude analyses we find that helicity flip amplitudes for both vector and tensor exchanges are consistent with being Reggelike. In this instance both Regge and geometrical-optical models give similar predictions for the imaginary part of the amplitude. Which interpretation provides the more fundamental understanding is a matter of opinion, however. For helicity nonflip amplitudes the situation is more confused. The imaginary parts of the crossing odd amplitudes are consistent with being peripheral, but for the even amplitudes the analyses are in conflict. The real part of these amplitudes are generally unknown.

Assuming the DAM is qualitatively correct, we then find a consistent description of ρ and A_2 exchange data that suggests that duality and EXD are to be applied to peripheral Regge exchange amplitudes. K* and K** amplitudes are determined from an analysis of Λ^o and Σ data, and are found to be similar to the better understood ρ and A_2 amplitudes. The contribution of the K* and K** amplitudes disagrees with SU(3) predictions, however.

The data compilation of Λ and Σ data suggests that the s-u crossed reactions have equal forward differential cross sections, but that the slopes of the forward differential cross sections differ for the present range of experimental data, $3 \lesssim P_{LAB} \lesssim 15$ GeV/c.

5. Acknowledgements

I would like to thank Y. Avni, M. Davier, D. Leith and J. Loos for many interesting discussions involving subjects related to this talk. I wish also to thank D. Leith for his support and interest.

References:

1. H. Harari, Ann. Phys. (N.Y.) 63, 432 (1971); SLAC Report No. SLAC-PUB-837.

2. R. J. Cashmore and A. J. G. Hey, Phys. Rev. D6, 1303 (1972).

3. F. Halzen and C. Michael, Phys. Letters 36B, 367 (1971).

4. M. Davier and H. Harari, Phys. Letters 35B, 239 (1971).

5. A. B. Wicklund, I. Ambats, D. S. Ayres, R. Diebold, A. F. Greene, S. L. Kramer, A. Lesnik, D. R. Rust, C. E. W. Ward, and D. D. Yavonovich, Bull. Amer. Phys. Soc. 17, 126 (1972), and submitted to IVth International Conference on High Energy Collisions, Oxford (1972).

6. D. Cline and J. Matos, Nucl. Phys. B33, 421 (1971).

7. H. A. Gordon, K.-W. Lai and F. E. Paige, Phys. Rev. D5, 1113 (1972).

8. M. Davier, Phys. Letters 40B, 369 (1972).

9. G. Chadwick, Y. Eisenberg and E. Kogan, SLAC Report No. SLAC-PUB-1093.

10. V. Barger and F. Halzen, "Successes and Failures of Dual Absorption Models", Wisc. Preprint (1971).

11. V. Barger, K. Geer and F. Halzen, "The Structure of Elastic Scattering: Are Tensor Exchanges Peripheral?" Wisc. Preprint (1972).

12. H. J. Halpern, R. Prepost, D. H. Tompkins, R. L. Anderson, B. Gottschalk, D. B. Gustavson, D. M. Ritson, G. A. Weitsch and B. H. Wiik, SLAC Reports No. SLAC-PUB-1085 and SLAC-PUB-1086.

13. H. Harari, SLAC Report No. SLAC-PUB-914; Phys. Rev. Letters 26, 1400 (1971).

14. J. S. Loos and J. A. J. Matthews, SLAC Report No. SLAC-PUB-1068.

15. K.-W. Lai and J. Louie, Nucl. Phys. B19, 205 (1970).

16. R. Barloutaud, "Quasi Two Body and Two Body Inelastic Hadronic Interactions", IVth International Conference on High Energy Collisions, Oxford, (1972).

17. F. J. Gilman, J. Pumplin, A. Schwimmer, and L. Stodolsky, Phys. Letters 31B, 387 (1970); H. Harari and Y. Zarmi, Phys. Letters 32B, 291 (1970).

18. G. W. Brandenburg, A. D. Brody, W. B. Johnson, D. W. G. S. Leith, J. S. Loos, G. J. Luste, J. A. J. Matthews, K. Moriyasu, B. C. Shen, W. M. Smart, F. C. Winkelmann and R. J. Yamartino, Nucl. Phys. B45, 397 (1972).

19. Aachen-Berlin-Bonn-CERN-Heidelburg Collaboration, J. V. Beaupre et al, CERN Report No. CERN/D.Ph II/PHYS 72-17.

20. J. V. Allaby, AIP Conference Proceedings (Irvine Conference - 1971), Ed. M. Bander, G. L. Shaw and D. Y. Wong, Amer. Instit. of Phys., New York (1972).

21. H. Alvensleben et al, Phys. Rev. Letters 28, 66 (1972); A-B-B-H-H-M Collaboration, Phys. Rev. 175, 1669 (1968); and ibid, 188, 2060 (1969).

22. See ref. 9 for references to old $\gamma p \rightarrow \phi p$ data.

23. V. Barger and D. Cline, Phys. Rev. Letters 24, 1313 (1970).

24. See for example the data of W. de Baere et al, Il Nuovo Cimento 45A, 885 (1966); V. Chabaud et al, Phys. Letters 38B, 445 (1972).

25. S. P. Denisov, S. V. Donskov, Y. P. Gorin, A. I. Petrukhin, Y. D. Prokoshkin, D. A. Stoyanova, J. V. Allaby, and G. Giacomelli, Phys. Letters 36B, 415 (1971)

26. T. Lasinski, R. Levi Setti, R. Schwarzschild, and P. Ukleja, Nucl. Phys. B37, 1 (1972).

27. V. Barger, K. Geer, and R. J. N. Phillips, "pp Slope Break and the Pomeron Periphery", Rutherford Report No. RPP/T/12.

28. Y. Zarmi, Phys. Rev. D4, 3455 (1971).

29. V. Barger and R. J. N. Phillips, Phys. Rev. 187, 2210 (1969); H. Harari and Y. Zarmi, Phys. Rev. 187, 2230 (1969); R. Dolen, D. Horn and C. Schmidt, Phys. Rev. 168, 1766 (1968).

30. R. J. N. Phillips, "Regge Cuts and Related Topics", Amsterdam International Conference on Elementary Particles (1971).

31. F. Uchiyama and J. S. Loos, Particle Data Group Report No. LBL-55; A. D. Brody, W. B. Johnson, B. Kehoe, D.W.G.S. Leith, J. S. Loos, G. J. Luste, K. Moriyasu, B. S. Shen, W. M. Smart, F. C. Winkelmann, and R. J. Yamartino, Phys. Rev. Letters 26, 1050 (1971).

32. G. Höhler and R. Strauss, Karlsruhe Report, (1971).

33. H. Harari and A. Schwimmer, Phys. Rev. D5, 2780 (1972).

34. Results submitted to the 16th International Conference on High Energy Physics, Batavia 6 - 13 Sept. 1972 by R. J. Miller, K. Paler, J. J. Phelan, T. P. Shah, B. Chaurand, B. Drevillon, G. Labrosse, R. Lestienne, D. Linglin, R. A. Salmeron, R. Barloutaud, A. Borg, C. Lauedec, F. Pierre, and M. Spiro, "Two Body Final States in K^-p Interactions at 14.3 GeV/c" do infact agree with the curves on fig. 19, yielding a slope of $B = 5.6 \pm 1.0$ for $K^-p \rightarrow \pi^0\Lambda^0$ at 14.3 GeV/c.

35. H. Harari, Phys. Rev. Letters 22, 562 (1969); J. L. Rosner, ibid 22, 689 (1969).

36. V. Barger and A.D. Martin, Phys. Letters 39B, 379 (1972).

Figures

1. Differential Cross Sections at 5 GeV/c for $Xp \rightarrow Xp$ and $\bar{X}p \rightarrow \bar{X}p$ from ref. 5.
2. Differential cross sections for $K^o p \rightarrow Q^o p$ and $\bar{K}^o p \rightarrow \bar{Q}^o p$ in the momentum interval $4 \leq P_{LAB} \leq 12$ GeV/c from ref. 18.
3. Separation of the imaginary part of the s-channel helicity nonflip amplitude as given in Eqn. (5). The analysis is at 5 GeV/c from ref. 4.
4. Legendre coefficients, see ref. 4, for the amplitude shown in Fig. 3.
5. Separation of the real part of the s-channel helicity flip amplitude as given in Eqn. (9). The analysis is at 2.74 GeV/c from ref. 13.
6. Slope of the pomeron amplitude as a function of s determined from $\pi^{\pm}p$ elastic scattering data in ref. 8. The shaded region corresponds to the experimental slopes for the K^+p elastic scattering data.
7. (a) The "interaction radius" for f^o exchange as a function of s determined from $\pi^{\pm}p$ data in ref. 8, see Eqn. (13).
   (b) The slope parameter for f^o amplitude as a function of s.
8. Compilation of forward slopes for pp elastic scattering as a function of s from ref. 20.
9. (a) Slope parameter for f^o amplitude as a function of s determined from $\gamma p \rightarrow \rho^o p$ data in ref. 9, see Eqn. (15).
   (b) Slope of the pomeron amplitude as a function of s. The dashed line represents the results of Davier,[8] see Fig. 6. The shaded region estimates the slope of the pomeron from $\gamma p \rightarrow \phi p$ data of Ritson, Prepost et al[12] as discussed in the caption for Fig. 10.
10. (a) Experimental results for $\gamma p \rightarrow \phi p$ differential cross section at 12 GeV from ref. 12. The range of slopes corresponding to the dashed and solid curves are shown in Fig. 9.
    (b) Same data as in (a) but showing also Cornell and DESY results (ref. 21).

11. Differential cross section at $-t = 0.6$ GeV^2 as a function of s for $\gamma p \to \phi p$ from ref. 12.

12. f^o and pomeron residues evaluated from $\pi^{\pm} p$ elastic scattering data assuming energy independent rates of shrinkage for the pomeron between $\alpha'_p=0$ and $\alpha'_p=1.0$ GeV^{-2}. The analysis is from ref. 11.

13. Location of the first zeros in the contribution of prominent resonances to the s-channel helicity nonflip, f_{++}, and helicity flip, f_{+-}, amplitudes from ref. 13.

14. Comparison of the DAM results to the differential cross section data for (a) $\pi^- p \to \pi^o n$ and (b) $\pi^- p \to \eta^o n$ from ref. 14.

15. Comparison of the DAM results to the polarization data for (a) $\pi^- p \to \pi^o n$ and (b) $\pi^- p \to \eta^o n$ in the momentum interval 3.6 - 18.2 GeV/c from ref. 14.

16. S-channel helicity amplitudes evaluated at 6 GeV/c from DAM comparison to the data for (a) $\pi^- p \to \pi^o n$ and (b) $\pi^- p \to \eta^o n$ from ref. 14. The solid (open) points in (a) are from the analysis of Halzen and Michael (ref. 3) for the real (imaginary) parts of the s-channel amplitudes.

17. Compilation of cross sections for (a) $\bar{K}N \to \pi\Lambda$ and $\pi N \to K\Lambda$ and (b) $\bar{K}N \to \pi\Sigma$ and $\pi N \to K\Sigma$ channels from ref. 16. The curves on these data are not meant to be fits, but correspond to $\alpha_{eff}(0) \sim 0.25$.

18. Differential cross section extrapolated to t=0 for $\pi N \to K\Lambda^o$ and $\bar{K}N \to \pi\Lambda^o$. The curve is the DAM comparison to the data from ref. 14.

19. Slopes for the forward differential cross sections for $\pi N \to K\Lambda^o$ and $\bar{K}N \to \pi\Lambda^o$. The curves are the comparison of the DAM to the data for theoretical slopes calculated in the momentum transfer intervals: $A(0 \leq -t \leq 0.3$ GeV$^2)$; and $B(0.1 \leq -t \leq 0.4$ GeV$^2)$ from ref. 14. The $K^- p \to \pi^o \Lambda^o$ data at 14.3 GeV/c (*) comes from ref. 34.

20. Comparison of differential cross sections at ~ 4 GeV/c for (a) $K^- p \rightarrow \pi^- \Sigma^+$ and $\pi^+ p \rightarrow K^+ \Sigma^+$. The solid (dashed) curves, denoted (I), are the comparison of the DAM to the data in the $\pi^+ p$ ($K^- p$) channels respectively. (b) $K^- p \rightarrow \pi^0 \Lambda^0$ and $\pi p \rightarrow K^0 \Lambda^0$. The solid and dashed curves represent two different DAM comparisons to the data. The analysis is from ref. 14.

21. Polarization for the reactions (a) $\pi^+ p \rightarrow K^+ \Sigma^+$ in the momentum interval 3-14 GeV/c, and (b) $K^- p \rightarrow \pi^- \Sigma^+$ at 3.95 GeV/c. The solid and dashed curves represent two different DAM comparisons to the data. The analysis is from ref. 14.

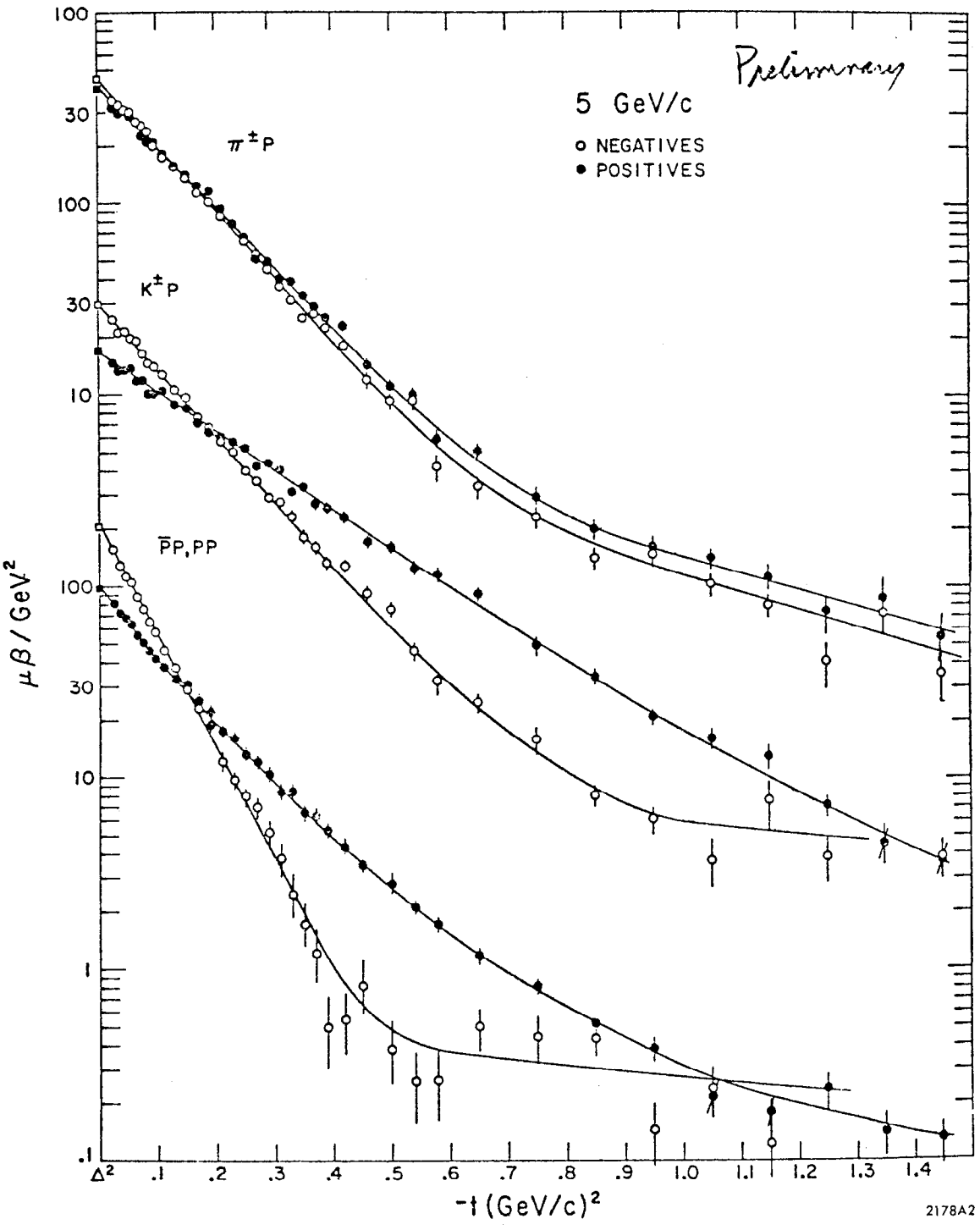
Preliminary
5 GeV/c
o NEGATIVES
• POSITIVES
$\pi^{\pm}P$
$K^{\pm}P$
$\bar{P}P, PP$
$\mu\beta$ / GeV^2
Δ^2
$-t$ (GeV/c)^2
2178A2

FIG. 1

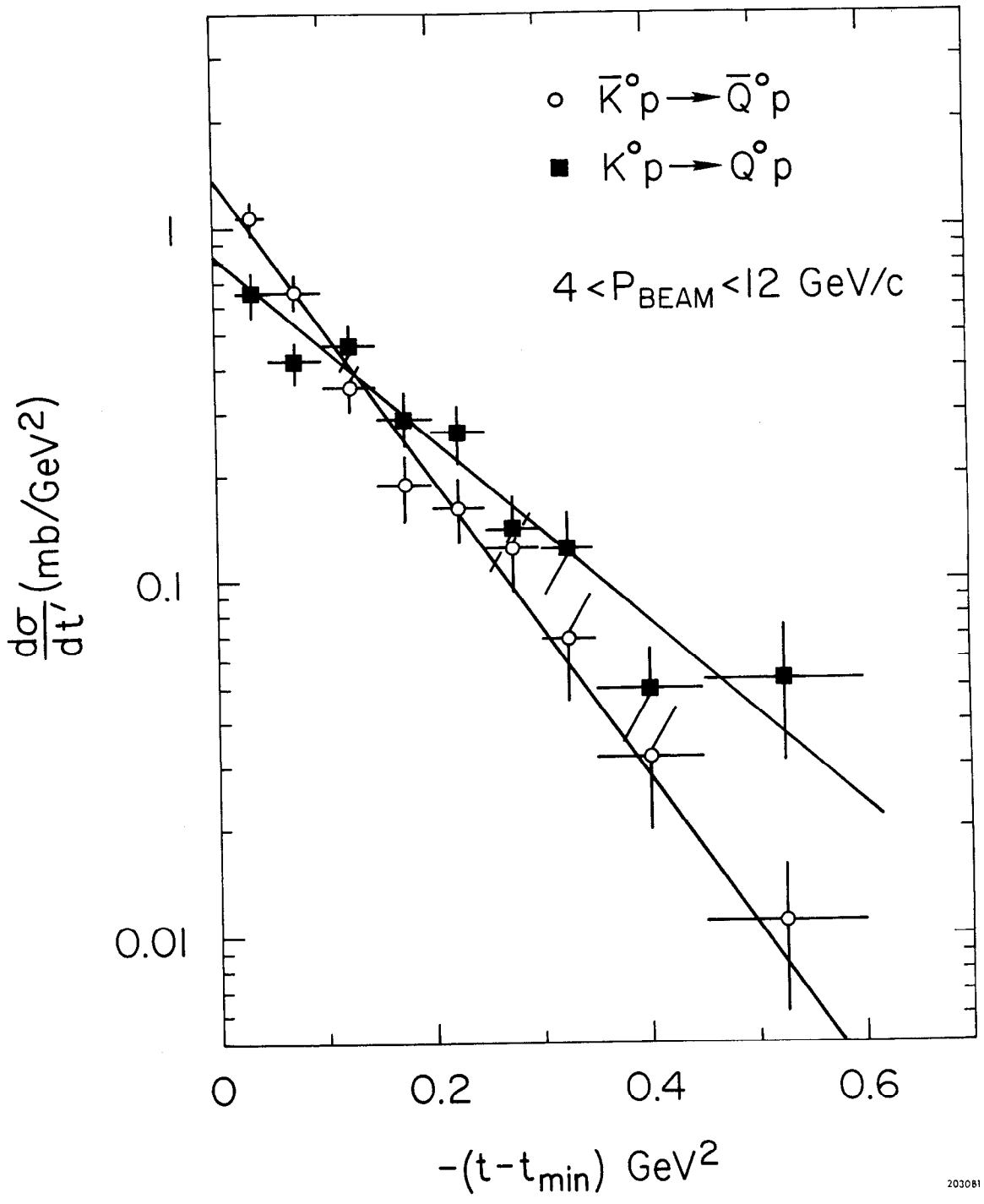
$\bar{K}^0p \rightarrow \bar{Q}^0p$
$K^0p \rightarrow Q^0p$
$4 < P_{BEAM} < 12$ GeV/c
$\frac{d\sigma}{dt'}$ (mb/GeV^2)
1
0.1
0.01
0
0.2
0.4
0.6
$-(t-t_{min})$ GeV^2
203081

FIG. 2

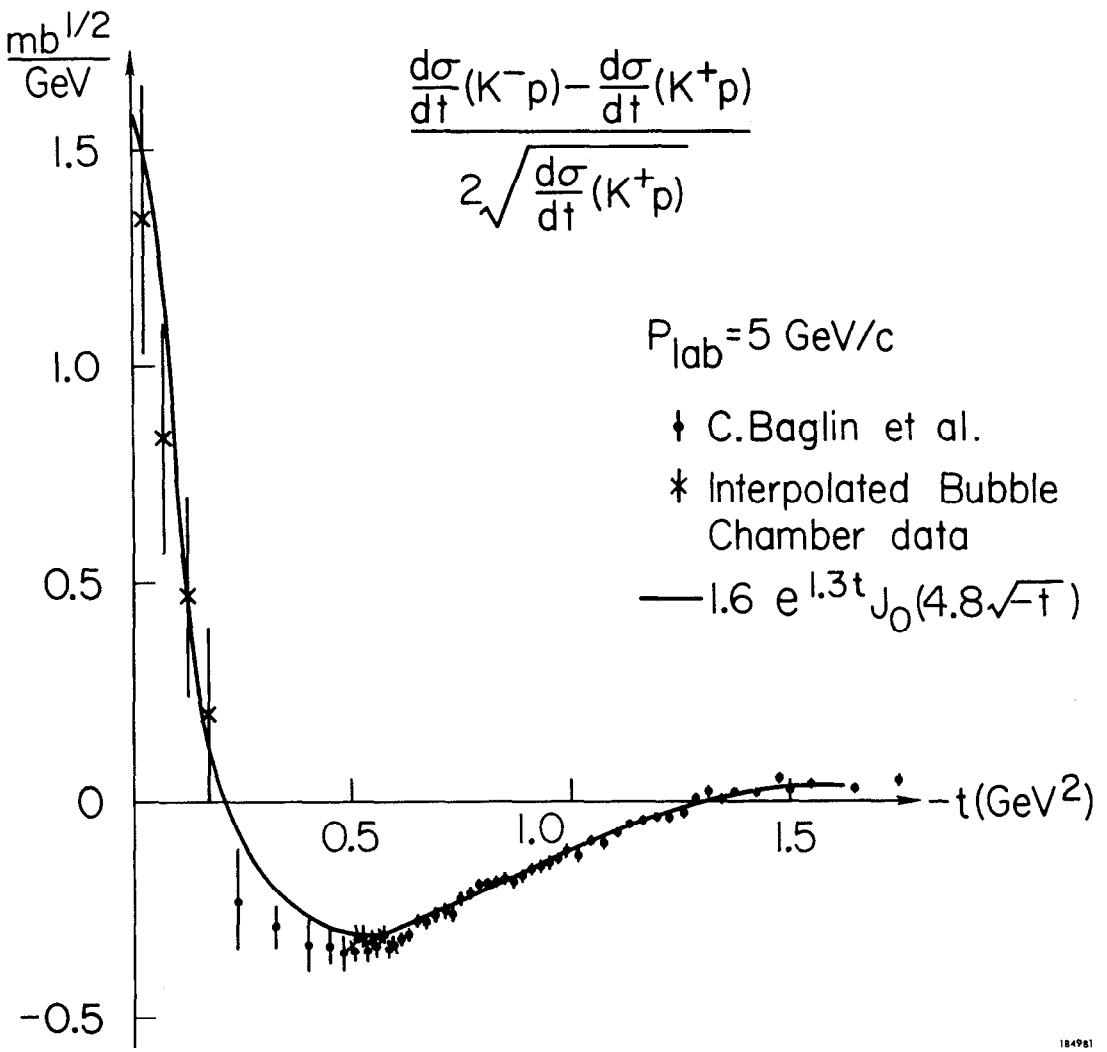
mb^1/2
GeV
1.5
1.0
0.5
0
-0.5
0.5
1.0
1.5
-t(GeV^2)
dσ/dt(K⁻p) − dσ/dt(K⁺p)
2√(dσ/dt(K⁺p))
P_lab = 5 GeV/c
C. Baglin et al.
Interpolated Bubble Chamber data
1.6 e^1.3t J0(4.8√-t)
184981

FIG. 3

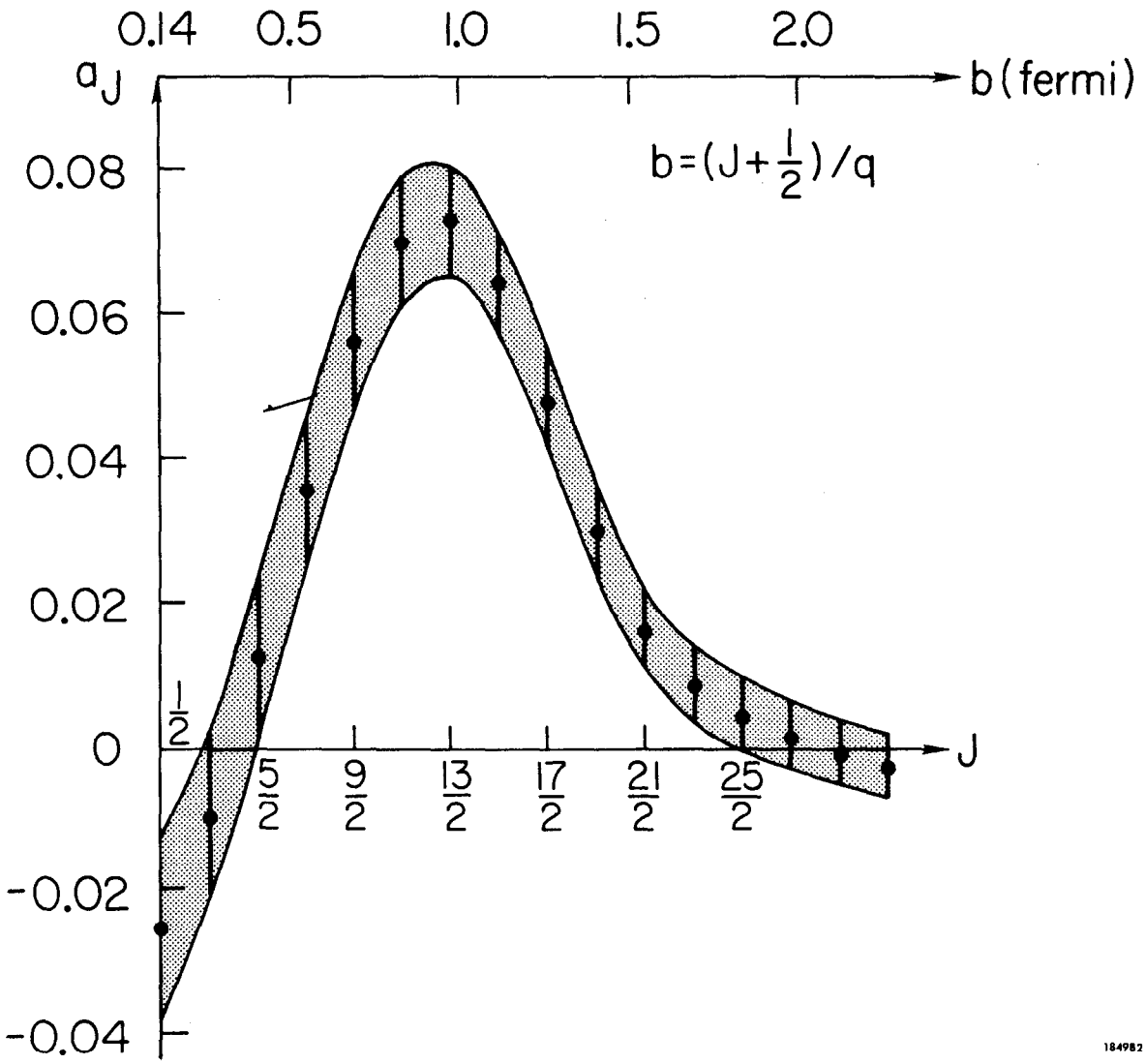
0.14
0.5
1.0
1.5
2.0
a_J
b (fermi)
$b=(J+\frac{1}{2})/q$
0.08
0.06
0.04
0.02
0
-0.02
-0.04
$\frac{1}{2}$
$\frac{5}{2}$
$\frac{9}{2}$
$\frac{13}{2}$
$\frac{17}{2}$
$\frac{21}{2}$
$\frac{25}{2}$
J
184982

FIG. 4

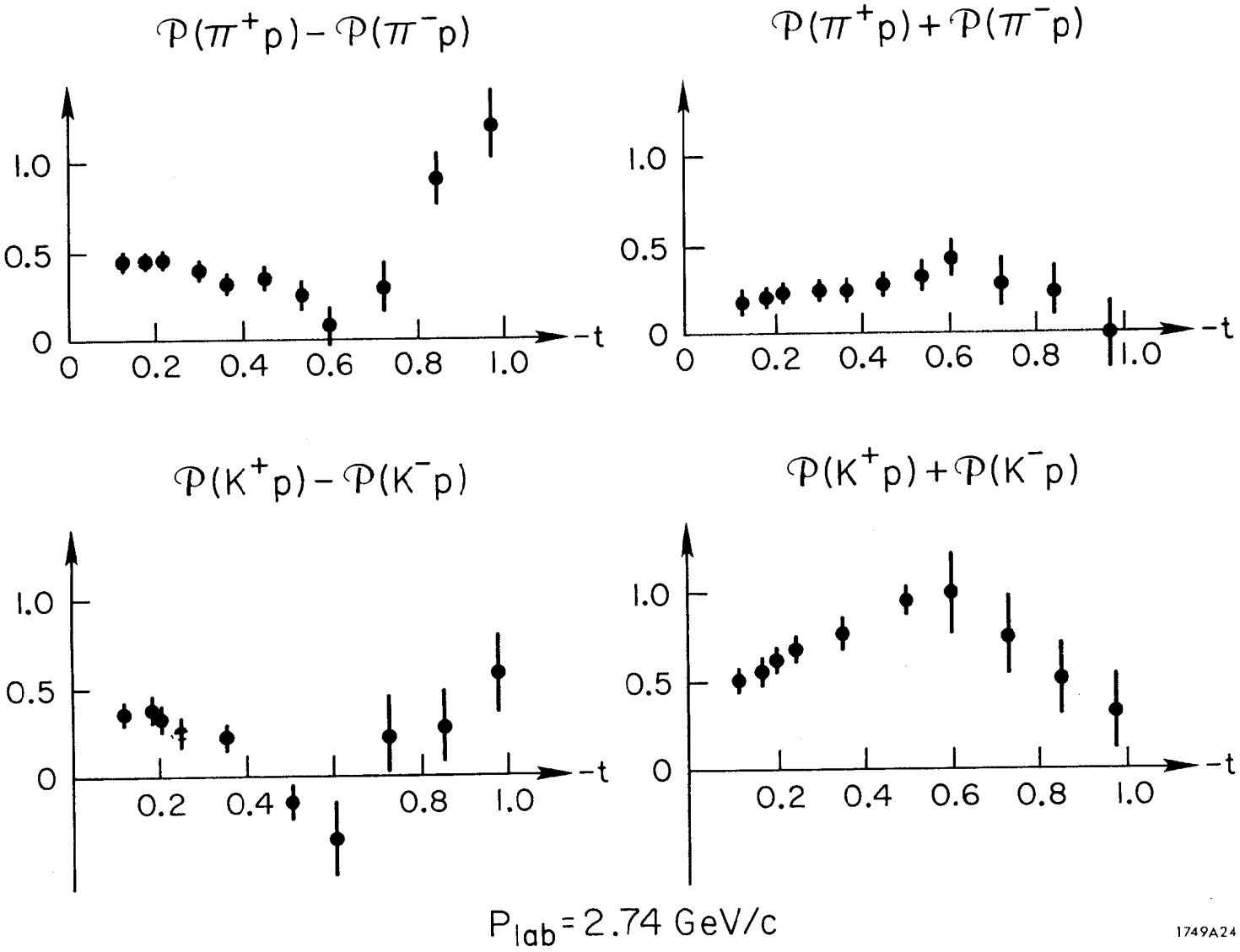
$\mathcal{P}(\pi^+p) - \mathcal{P}(\pi^-p)$
$\mathcal{P}(\pi^+p) + \mathcal{P}(\pi^-p)$
$\mathcal{P}(K^+p) - \mathcal{P}(K^-p)$
$\mathcal{P}(K^+p) + \mathcal{P}(K^-p)$
1.0
0.5
0
0.2
0.4
0.6
0.8
1.0
-t
$P_{lab} = 2.74$ GeV/c
1749A24

FIG. 5

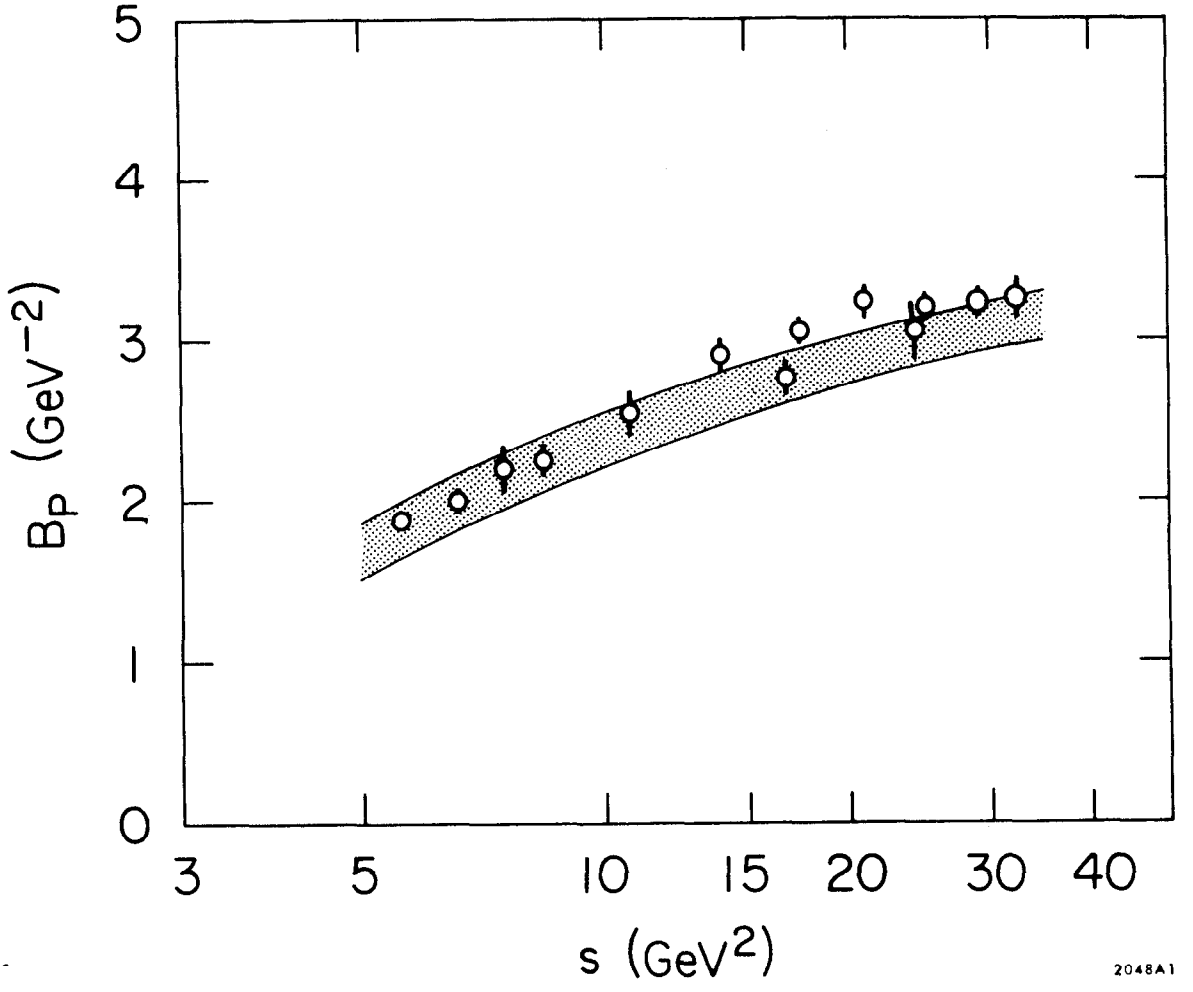

FIG. 6

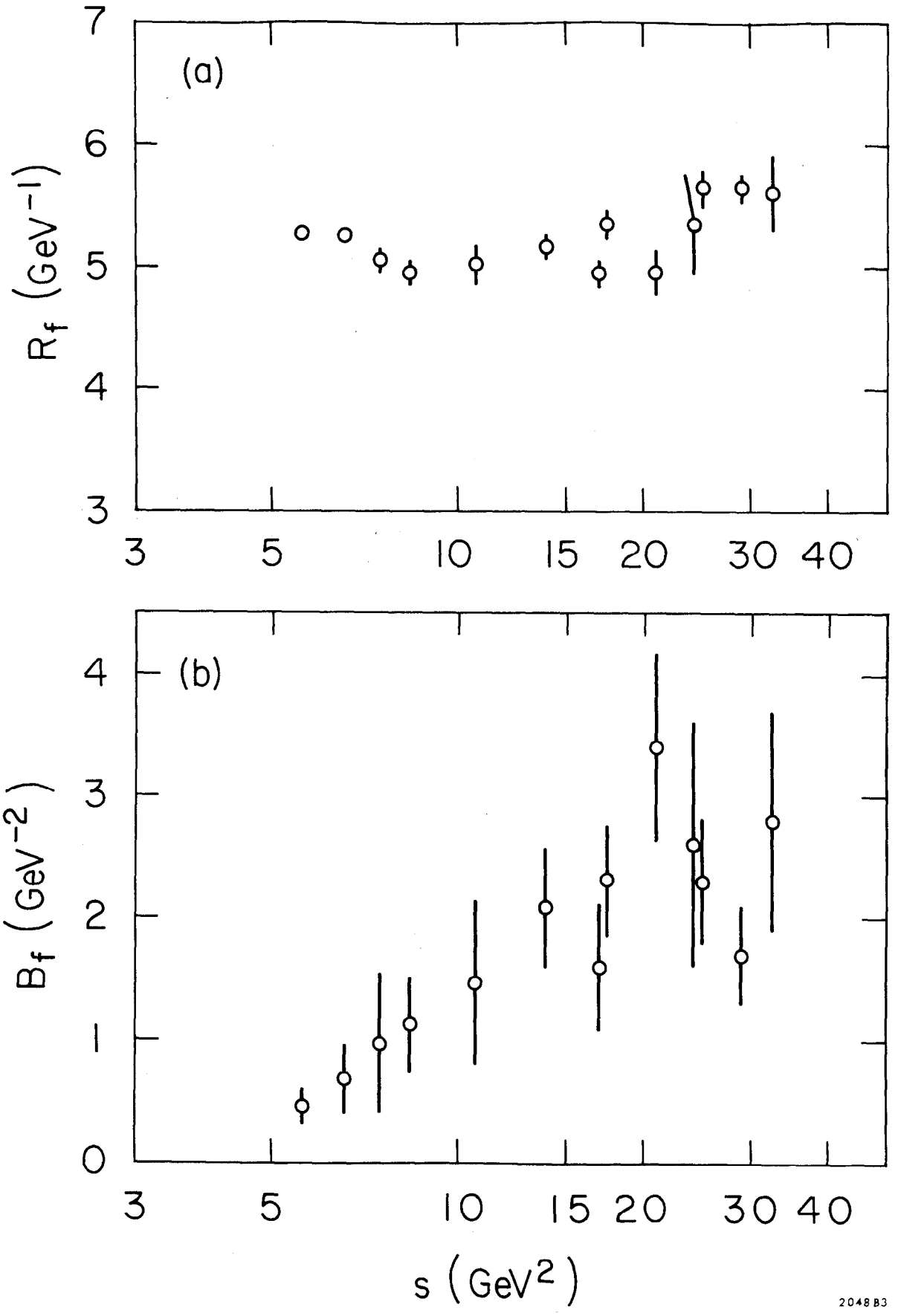
(a)
R_f (GeV^{-1})
7
6
5
4
3
3
5
10
15
20
30
40
(b)
B_f (GeV^{-2})
4
3
2
1
0
3
5
10
15
20
30
40
s (GeV^2)
2048B3

FIG. 7

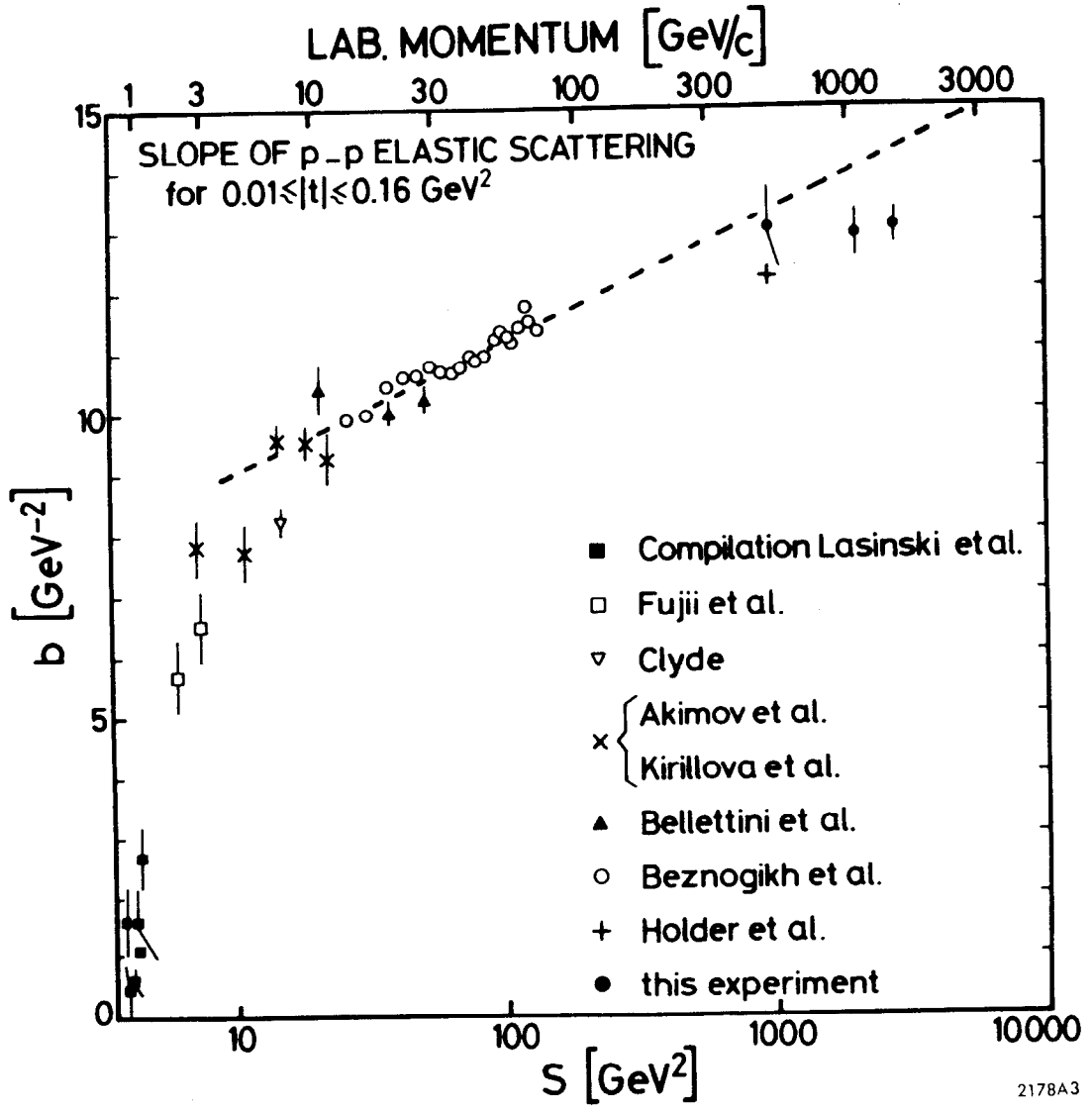
LAB. MOMENTUM [GeV/c]
1
3
10
30
100
300
1000
3000
SLOPE OF p-p ELASTIC SCATTERING
for 0.01≤|t|≤0.16 GeV²
b [GeV⁻²]
15
10
5
0
10
100
1000
10000
S [GeV²]
Compilation Lasinski et al.
Fujii et al.
Clyde
Akimov et al.
Kirillova et al.
Bellettini et al.
Beznogikh et al.
Holder et al.
this experiment
2178A3

FIG. 8

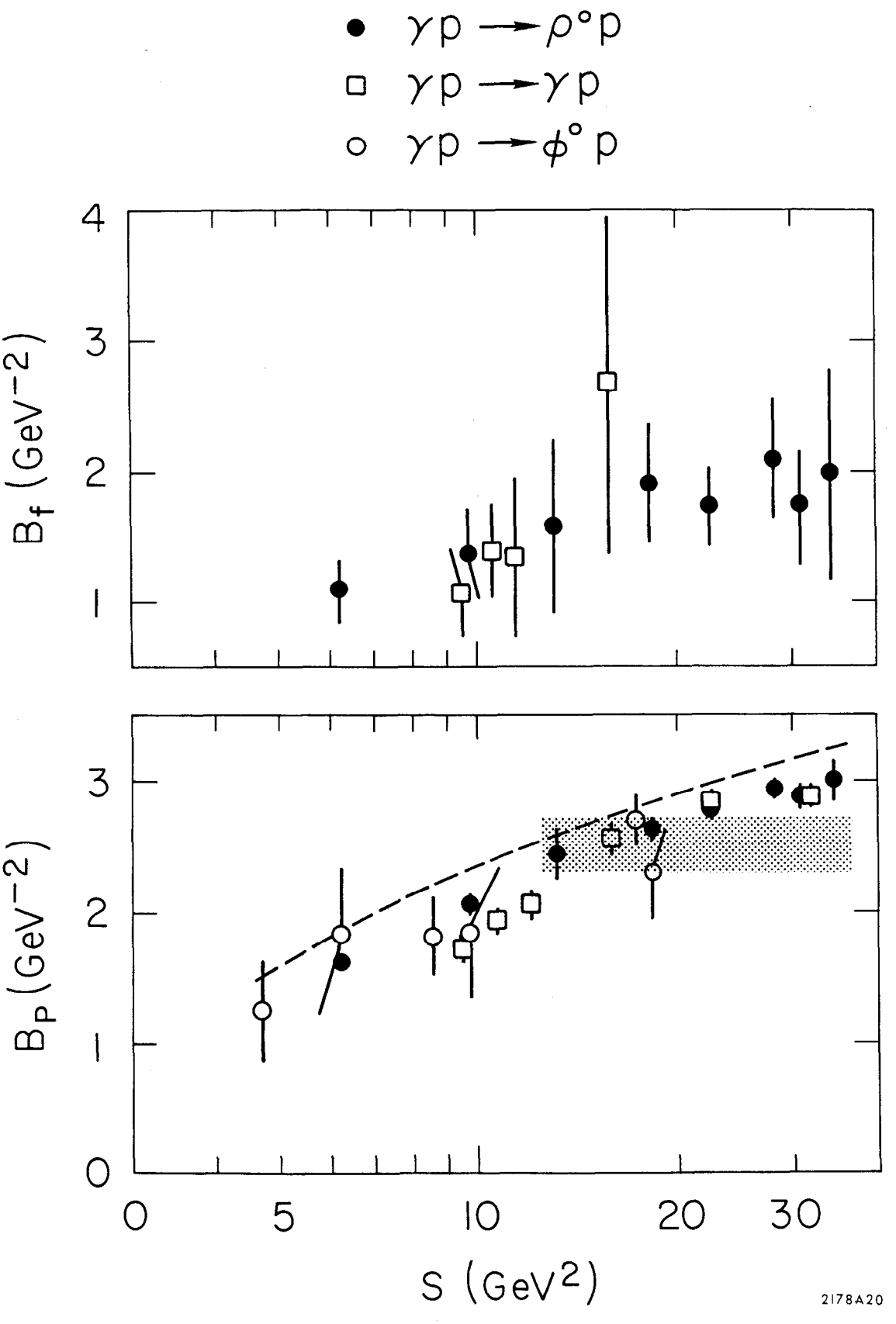

FIG. 9

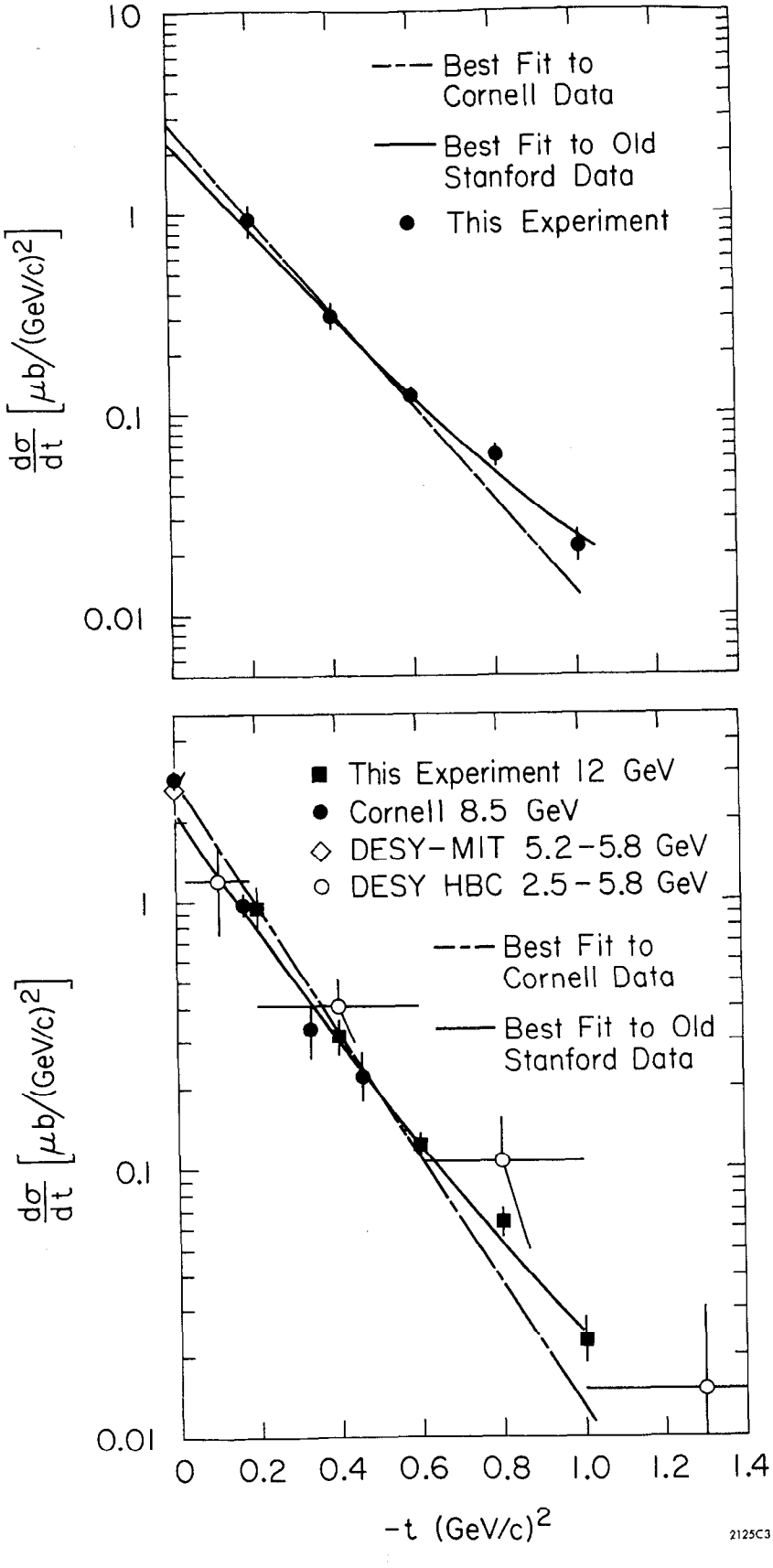
10
1
0.1
0.01
dσ/dt [μb/(GeV/c)²]
Best Fit to Cornell Data
Best Fit to Old Stanford Data
This Experiment
This Experiment 12 GeV
Cornell 8.5 GeV
DESY-MIT 5.2-5.8 GeV
DESY HBC 2.5-5.8 GeV
Best Fit to Cornell Data
Best Fit to Old Stanford Data
0
0.2
0.4
0.6
0.8
1.0
1.2
1.4
-t (GeV/c)²
2125C3

FIG. 10

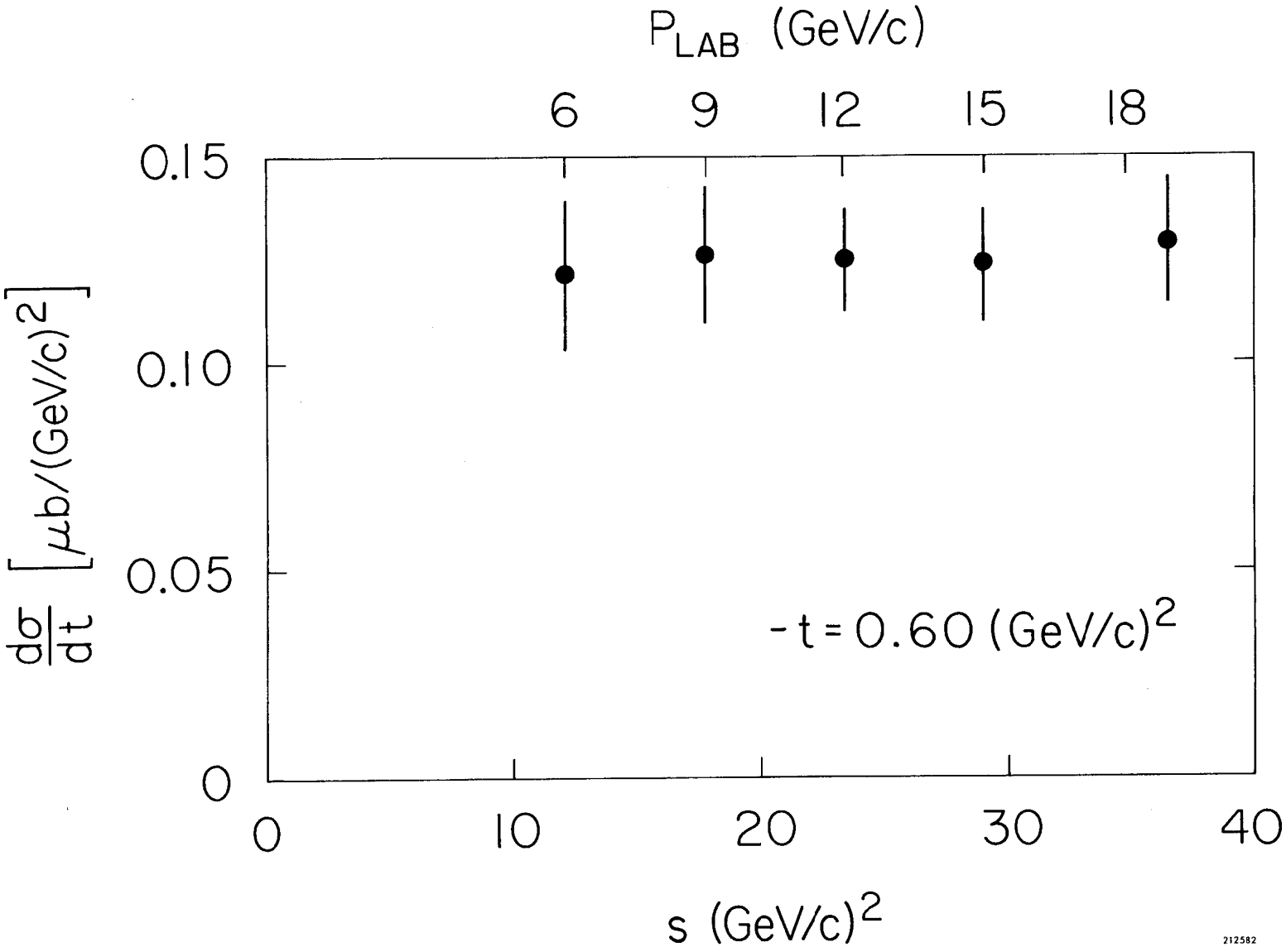
P_{LAB} (GeV/c)
6
9
12
15
18
0.15
0.10
0.05
0
$\frac{d\sigma}{dt}$ [μb/(GeV/c)^2]
$-t = 0.60$ (GeV/c)^2
0
10
20
30
40
s (GeV/c)^2
212582

FIG. 11

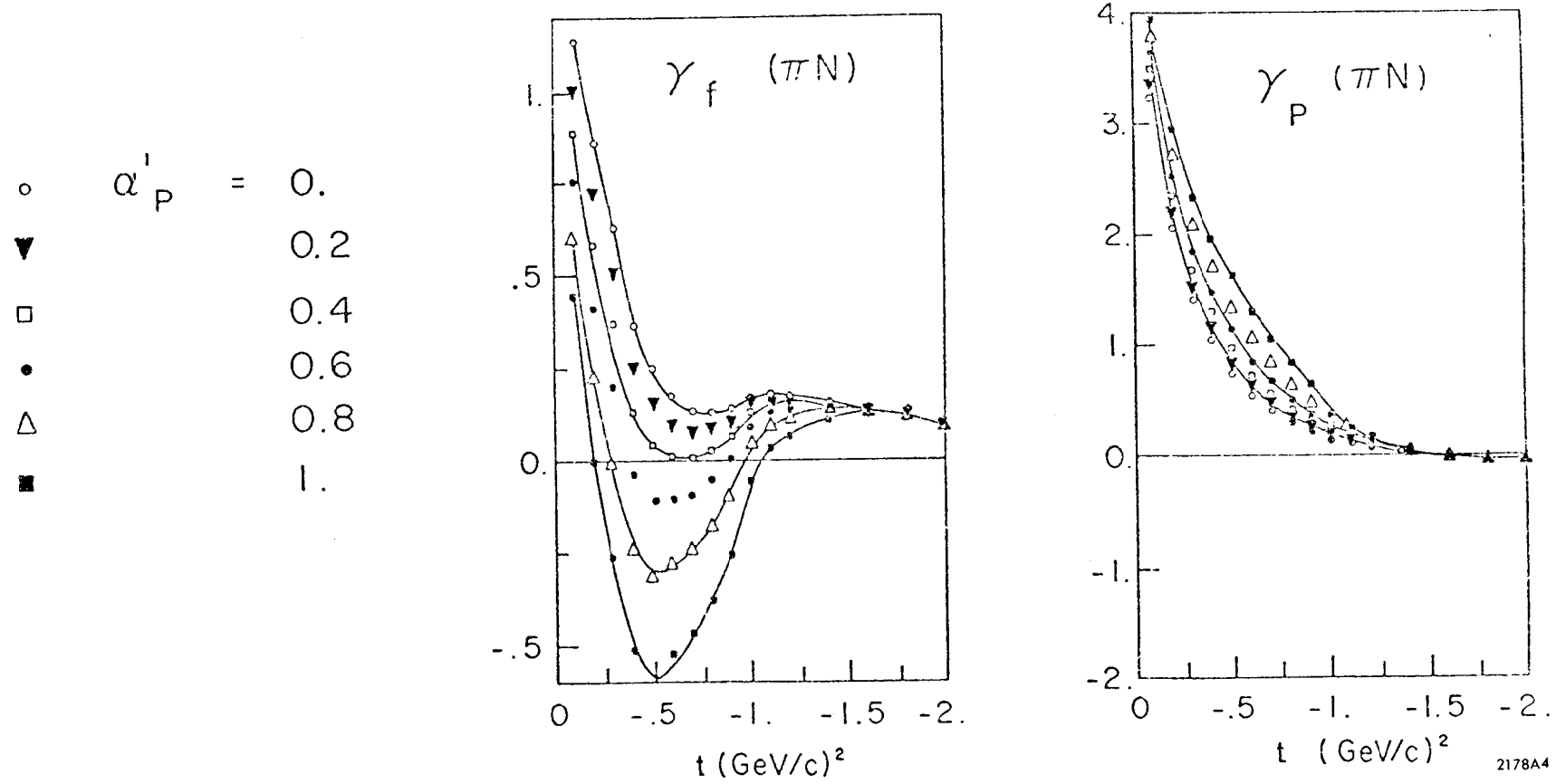
α'_P = 0.
0.2
0.4
0.6
0.8
1.
γ_f (πN)
1.
.5
0.
-.5
0
-.5
-1.
-1.5
-2.
t (GeV/c)^2
γ_P (πN)
4.
3.
2.
1.
0.
-1.
-2.
0
-.5
-1.
-1.5
-2.
t (GeV/c)^2
2178A4

FIG. 12

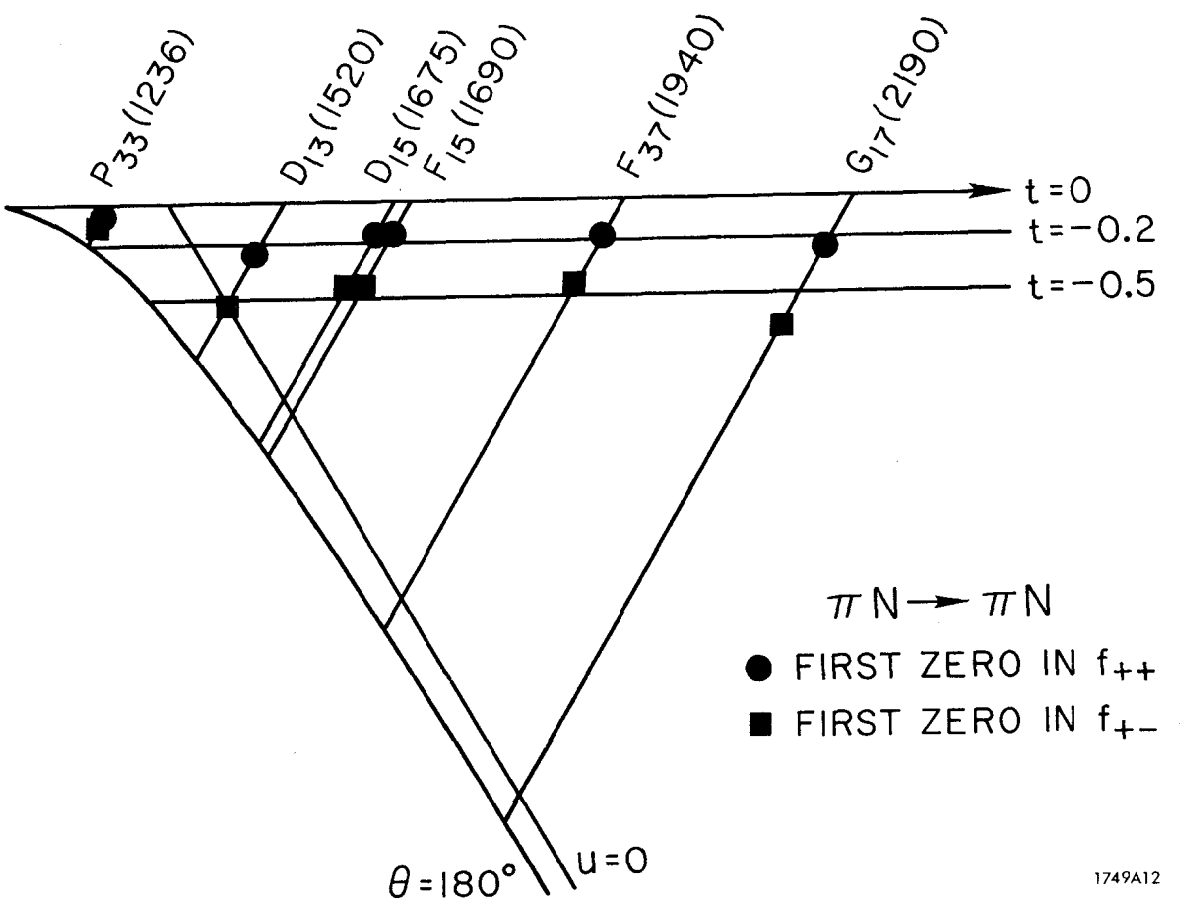
P33(1236)
D13(1520)
D15(1675)
F15(1690)
F37(1940)
G17(2190)
t=0
t=−0.2
t=−0.5
πN→πN
● FIRST ZERO IN f++
■ FIRST ZERO IN f+−
θ=180°
u=0
1749A12

FIG. 13

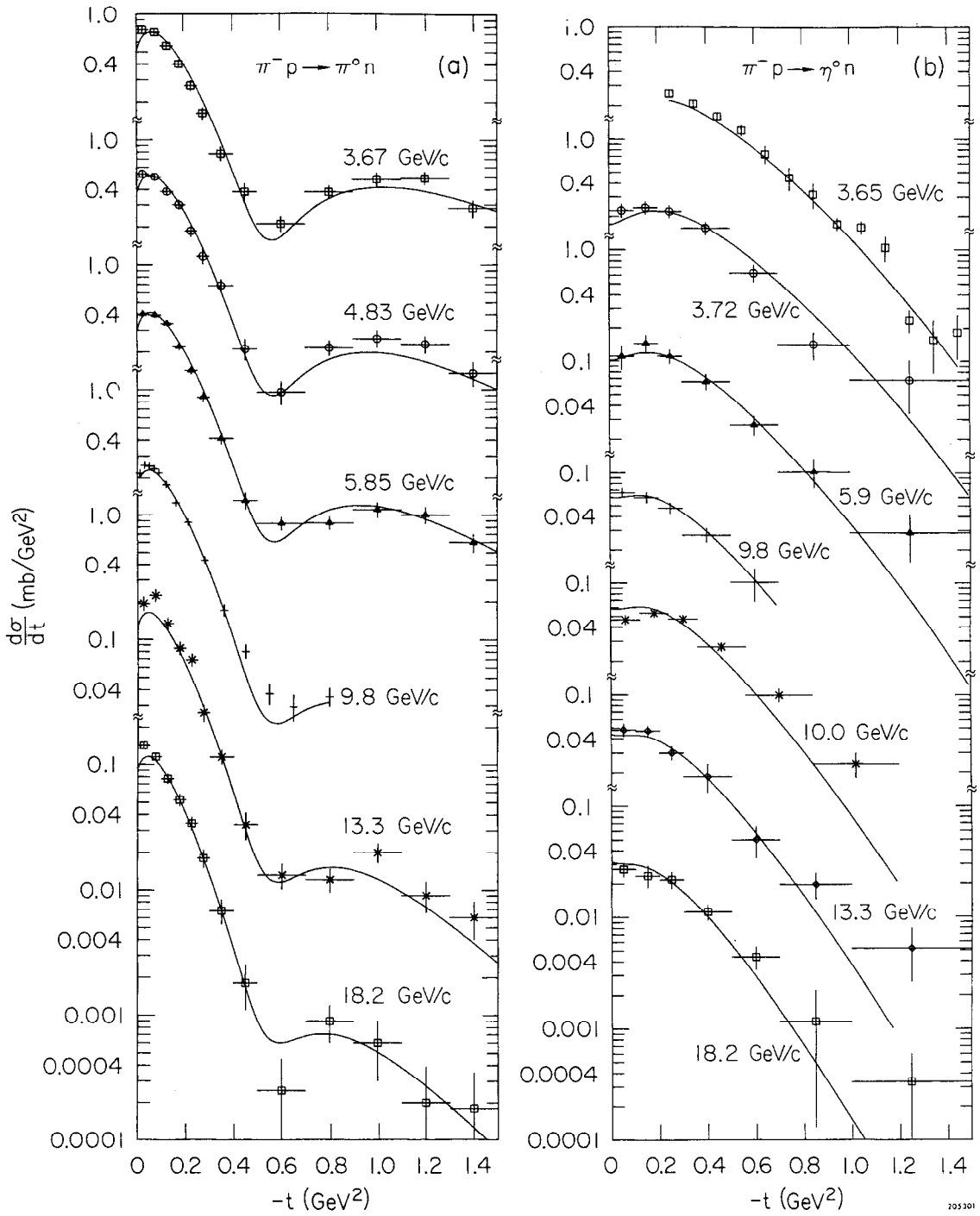
$\pi^- p \to \pi^\circ n$ (a)
3.67 GeV/c
4.83 GeV/c
5.85 GeV/c
9.8 GeV/c
13.3 GeV/c
18.2 GeV/c
$\pi^- p \to \eta^\circ n$ (b)
3.65 GeV/c
3.72 GeV/c
5.9 GeV/c
9.8 GeV/c
10.0 GeV/c
13.3 GeV/c
18.2 GeV/c
$\frac{d\sigma}{dt}$ (mb/GeV^2)
-t (GeV^2)
-t (GeV^2)
205301

FIG. 14

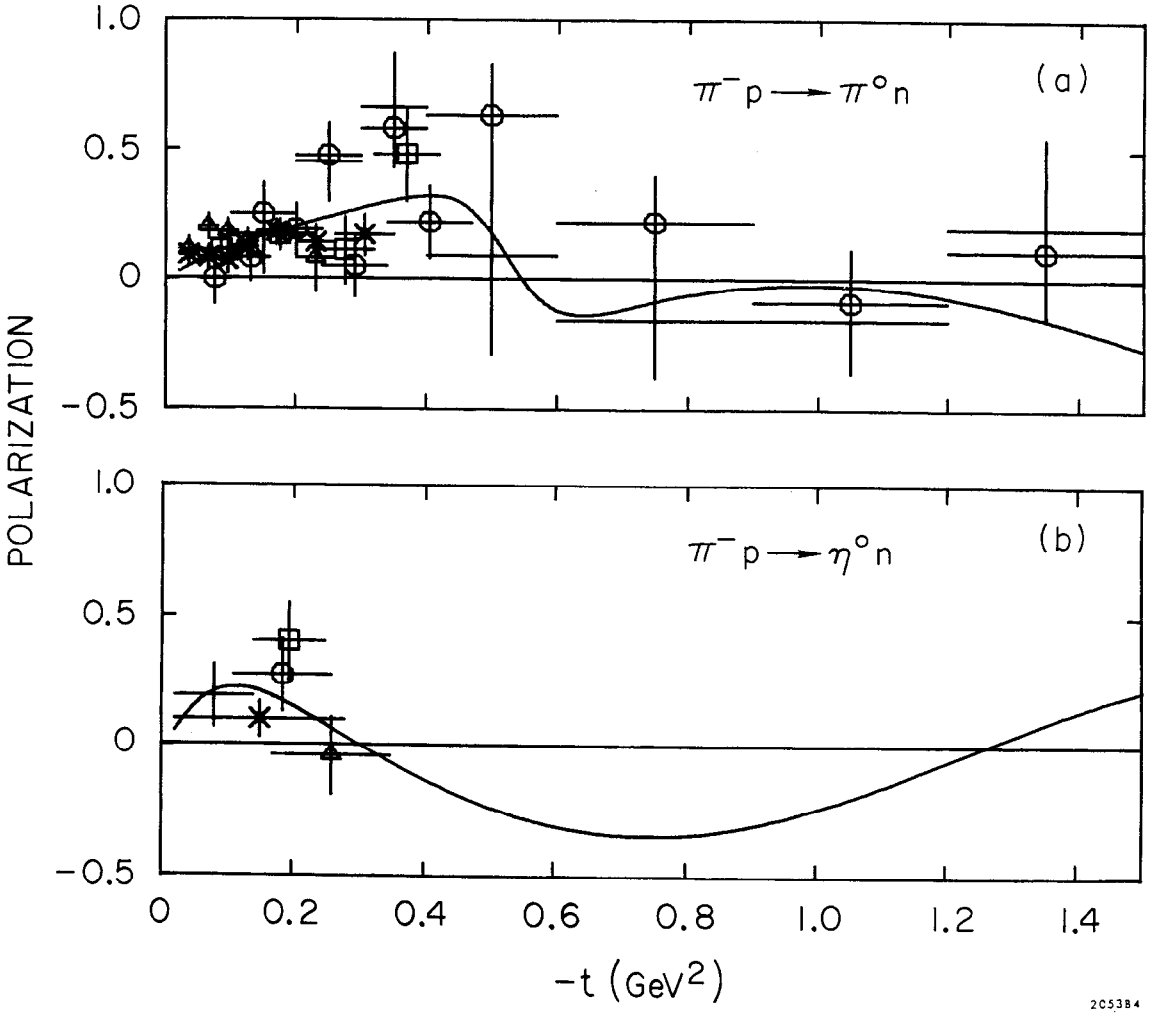
1.0
0.5
0
-0.5
POLARIZATION
$\pi^- p \rightarrow \pi^\circ n$
(a)
1.0
0.5
0
-0.5
$\pi^- p \rightarrow \eta^\circ n$
(b)
0
0.2
0.4
0.6
0.8
1.0
1.2
1.4
$-t\ (GeV^2)$
2053B4

FIG. 15

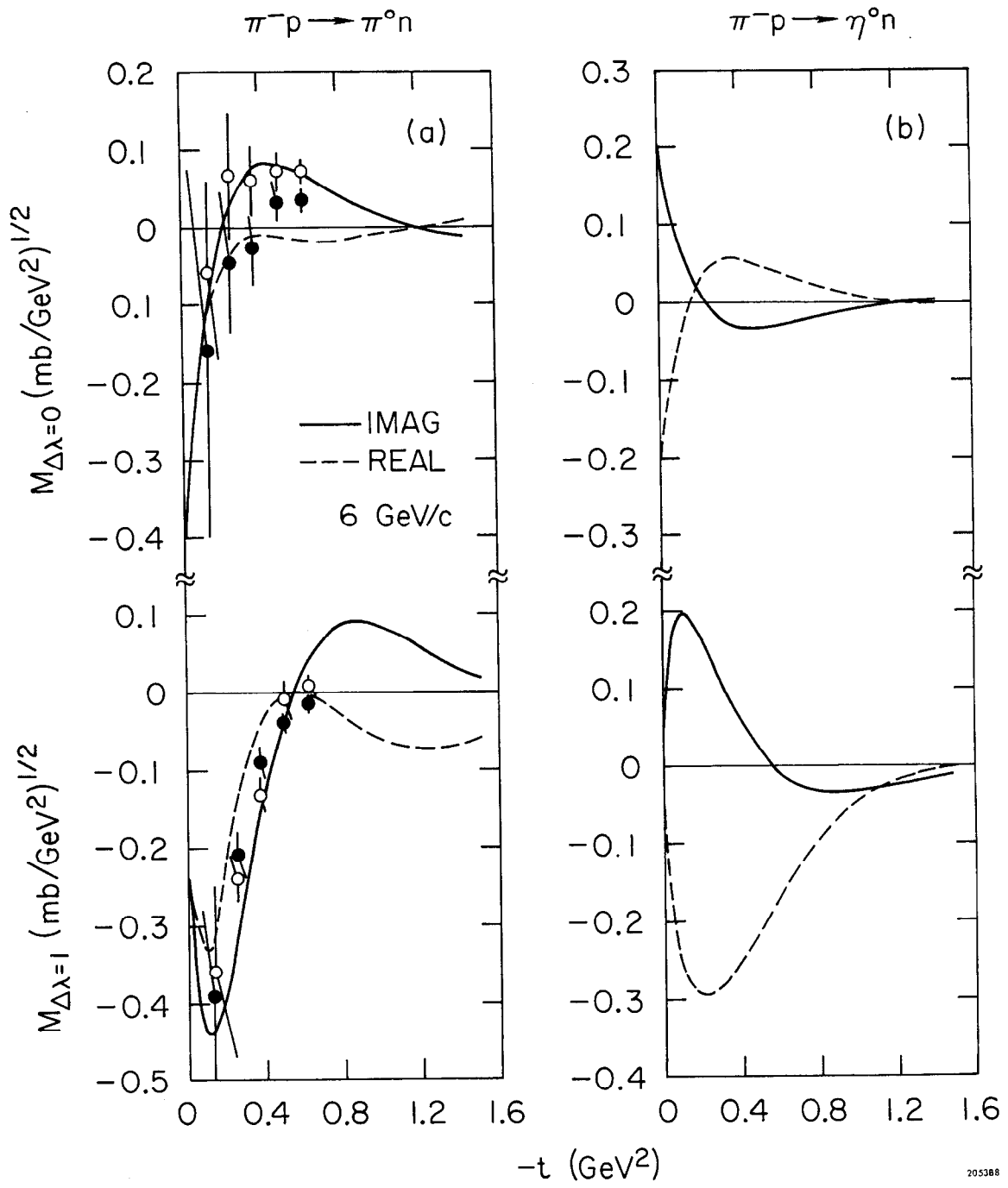
$\pi^- p \rightarrow \pi^0 n$
$\pi^- p \rightarrow \eta^0 n$
(a)
(b)
IMAG
REAL
6 GeV/c
$M_{\Delta\lambda=0}$ (mb/GeV^2)$^{1/2}$
$M_{\Delta\lambda=1}$ (mb/GeV^2)$^{1/2}$
$-t$ (GeV^2)
205388

FIG. 16

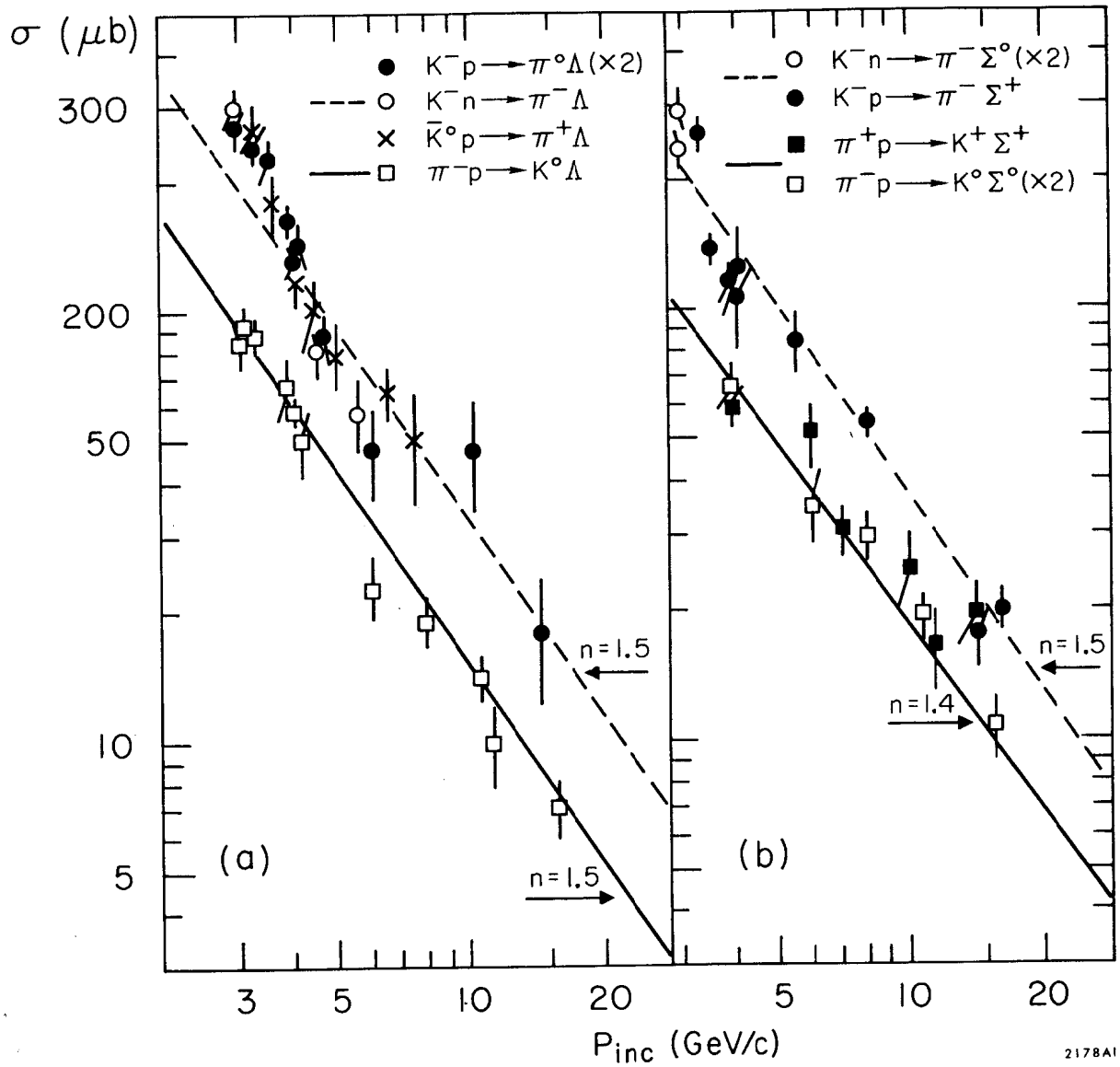
σ (μb)
300
200
50
10
5
K⁻p → π°Λ(×2)
K⁻n → π⁻Λ
K̄°p → π⁺Λ
π⁻p → K°Λ
n=1.5
n=1.5
(a)
3
5
10
20
K⁻n → π⁻Σ°(×2)
K⁻p → π⁻Σ⁺
π⁺p → K⁺Σ⁺
π⁻p → K°Σ°(×2)
n=1.5
n=1.4
(b)
5
10
20
Pinc (GeV/c)
2178A1

FIG. 17

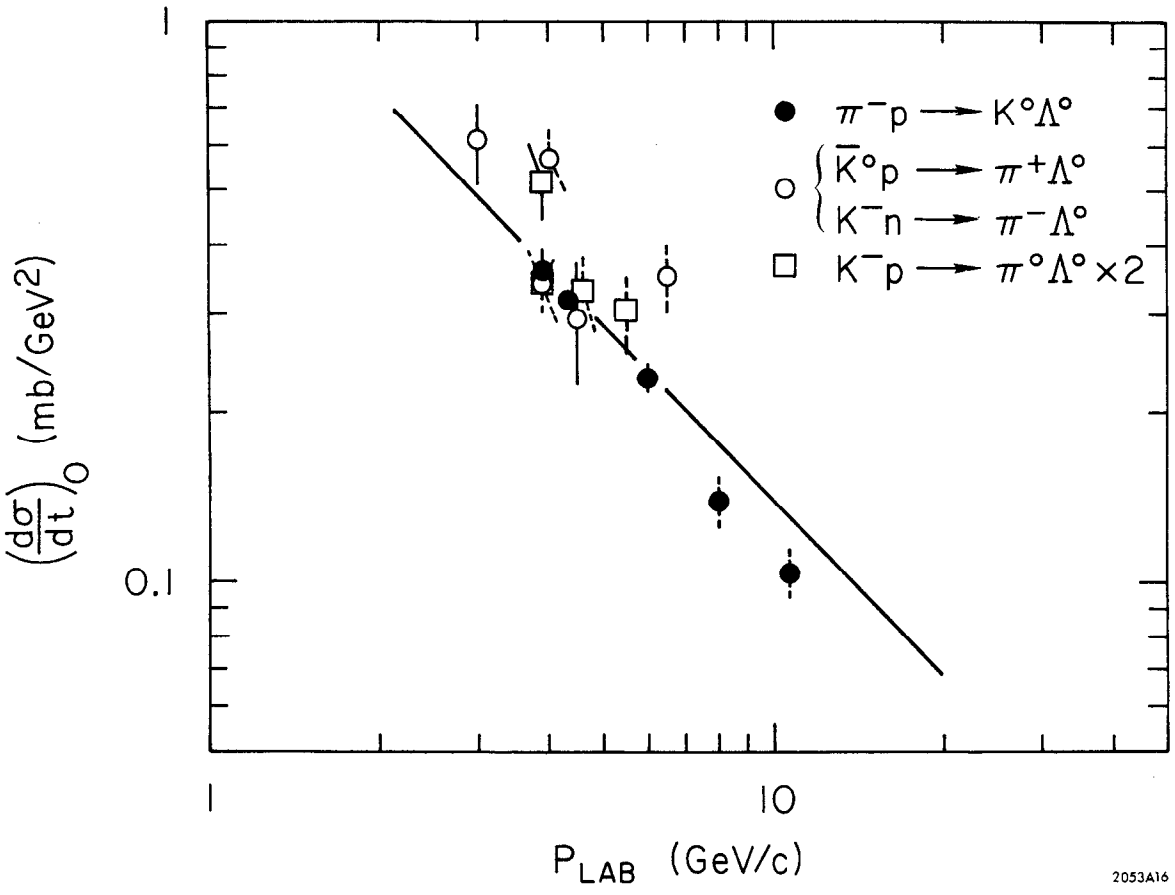
1
0.1
$\left(\frac{d\sigma}{dt}\right)_0$ (mb/GeV^2)
$\pi^- p \rightarrow K^\circ \Lambda^\circ$
$\bar{K}^\circ p \rightarrow \pi^+ \Lambda^\circ$
$K^- n \rightarrow \pi^- \Lambda^\circ$
$K^- p \rightarrow \pi^\circ \Lambda^\circ \times 2$
1
10
P_{LAB} (GeV/c)
2053A16

FIG. 18

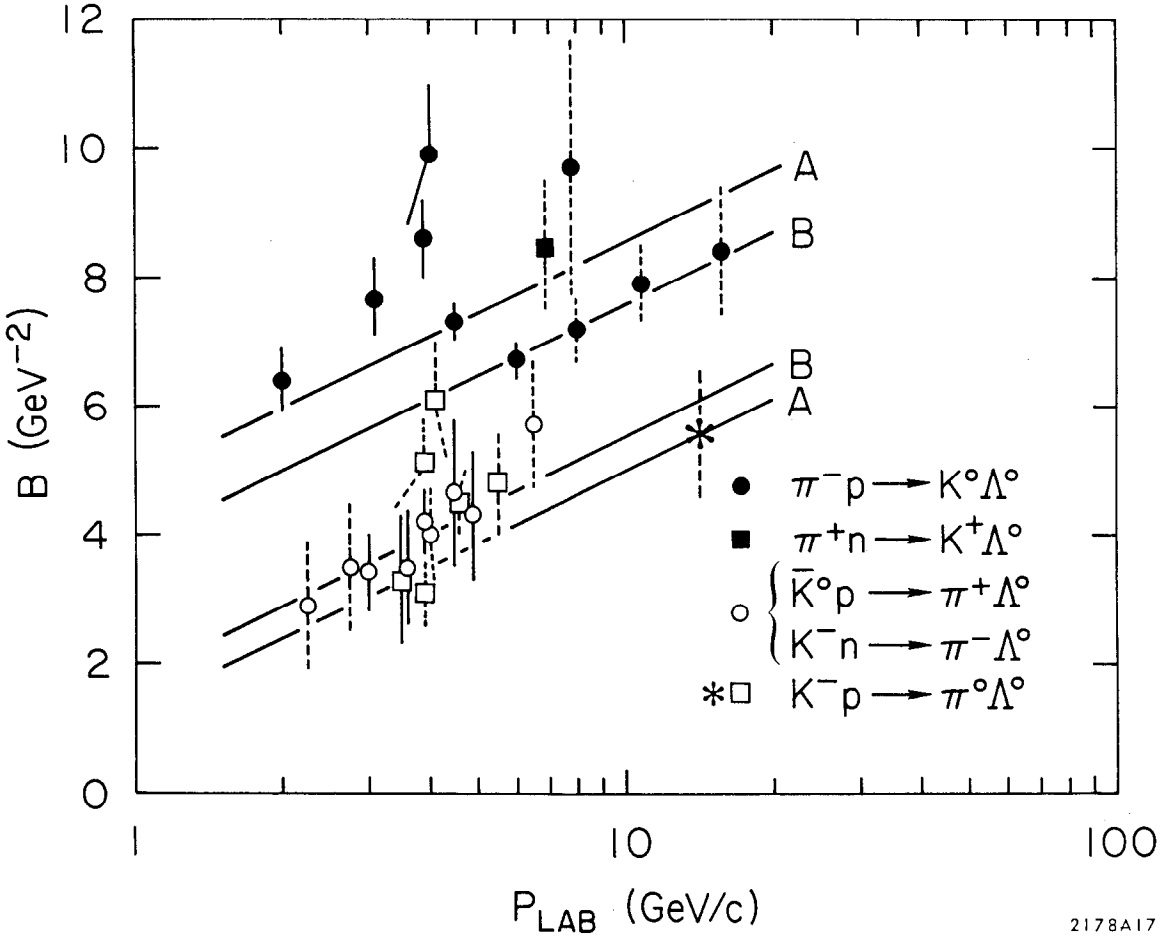
12
10
8
6
4
2
0
B (GeV^{-2})
1
10
100
P_{LAB} (GeV/c)
A
B
B
A
$\pi^- p \rightarrow K^\circ \Lambda^\circ$
$\pi^+ n \rightarrow K^+ \Lambda^\circ$
$\bar{K}^\circ p \rightarrow \pi^+ \Lambda^\circ$
$K^- n \rightarrow \pi^- \Lambda^\circ$
$K^- p \rightarrow \pi^\circ \Lambda^\circ$
2178A17

FIG. 19

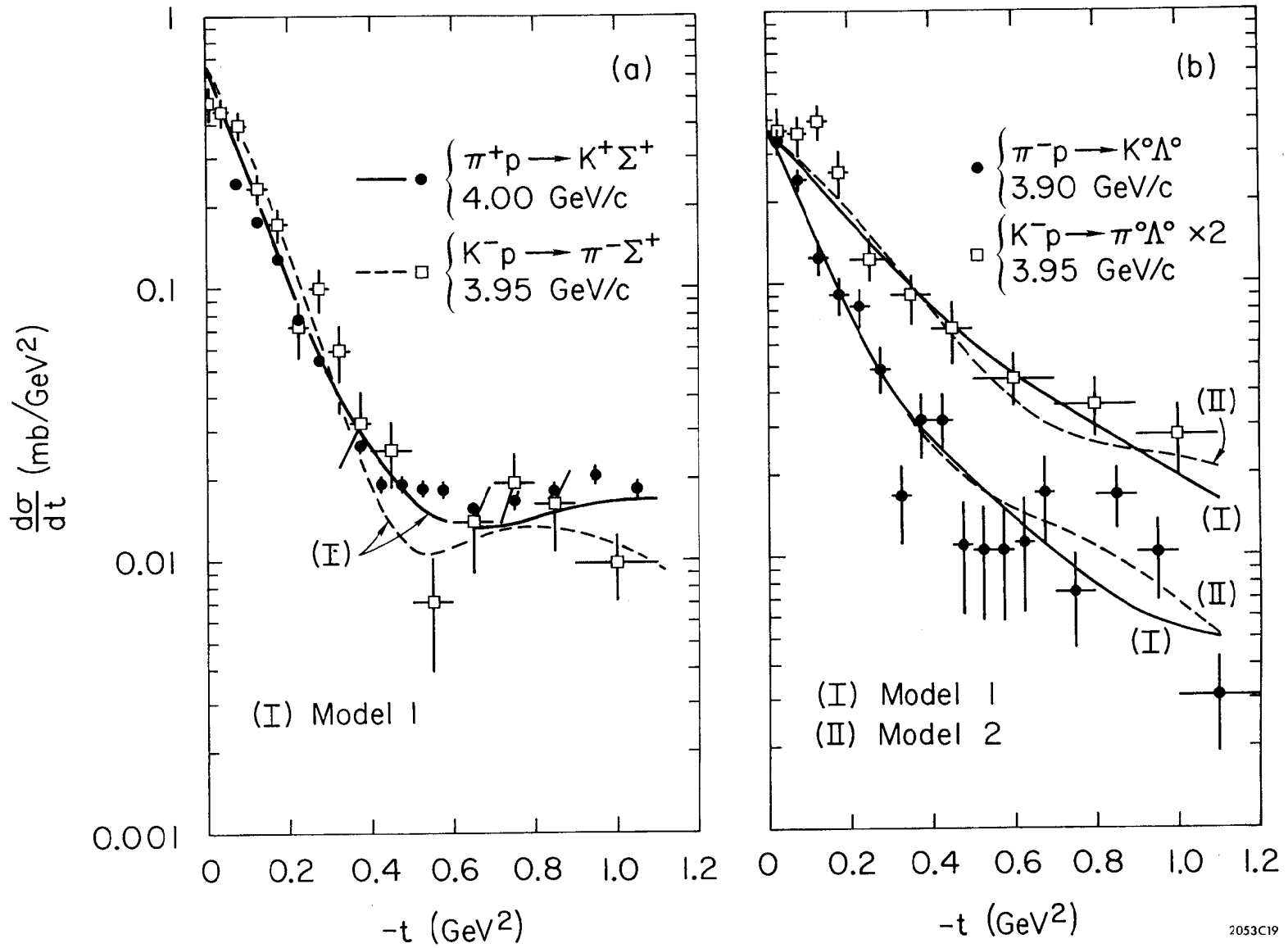
(a)
(b)
$\pi^+p \rightarrow K^+\Sigma^+$
4.00 GeV/c
$K^-p \rightarrow \pi^-\Sigma^+$
3.95 GeV/c
$\pi^-p \rightarrow K^\circ\Lambda^\circ$
3.90 GeV/c
$K^-p \rightarrow \pi^\circ\Lambda^\circ$ ×2
3.95 GeV/c
(I) Model 1
(II) Model 2
$\frac{d\sigma}{dt}$ (mb/GeV^2)
-t (GeV^2)
1
0.1
0.01
0.001
0
0.2
0.4
0.6
0.8
1.0
1.2
2053C19

FIG. 20

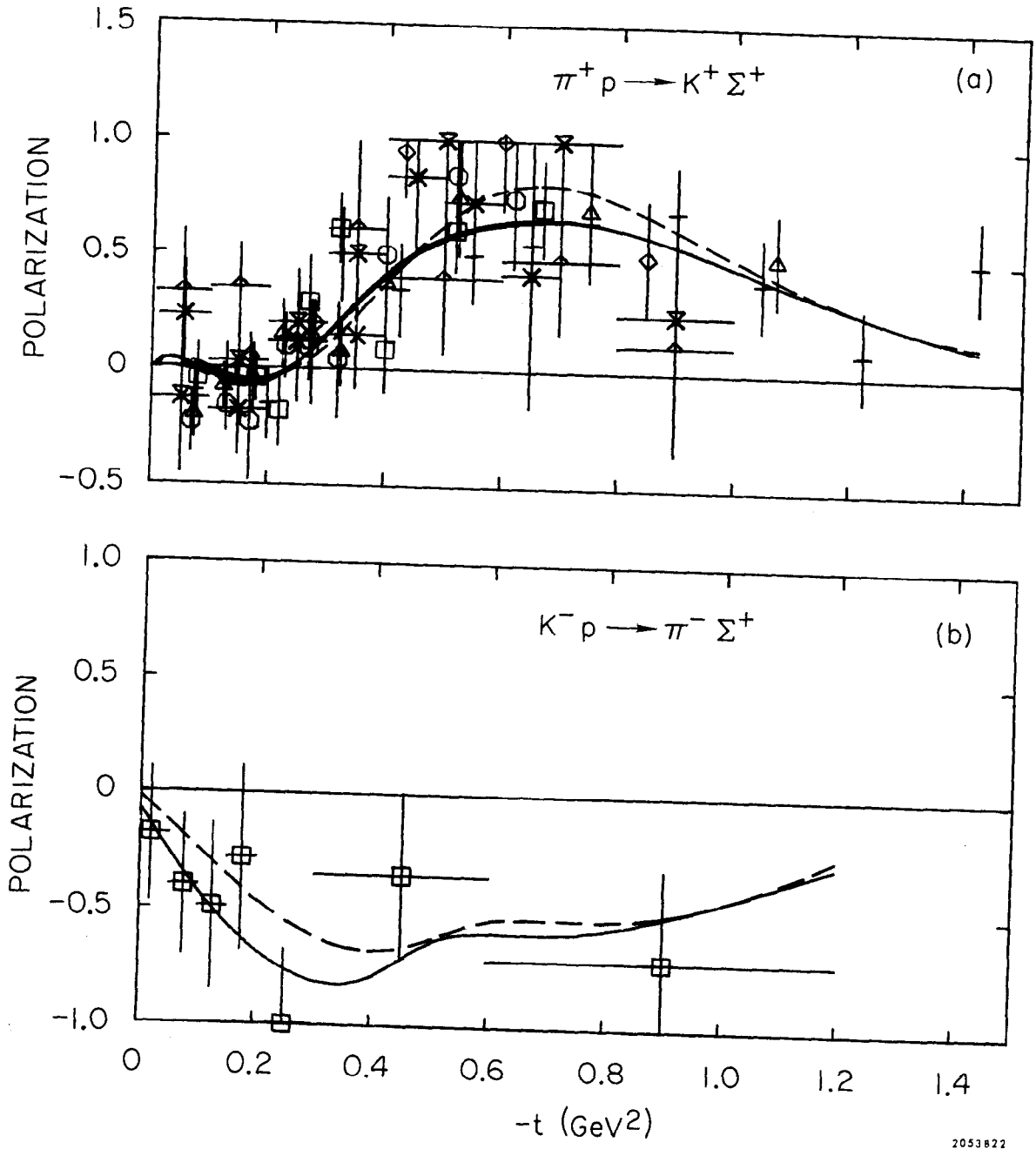
1.5
1.0
0.5
0
-0.5
POLARIZATION
$\pi^+ p \rightarrow K^+ \Sigma^+$
(a)
1.0
0.5
0
-0.5
-1.0
POLARIZATION
$K^- p \rightarrow \pi^- \Sigma^+$
(b)
0
0.2
0.4
0.6
0.8
1.0
1.2
1.4
$-t$ (GeV^2)
2053B22

FIG. 21